BULLETIN DE L'ASSOCIATION MINÉRALOGIQUE DU CANADA

THE CANADIAN MINERALOGIST

JOURNAL OF THE MINERALOGICAL ASSOCIATION OF CANADA

Volume 47 April 2009 Part 2

The Canadian Mineralogist
Vol. 47, pp. 233-262 (2009)
DOI: 10.3749/canmin.47.2.233

THE CRYSTAL CHEMISTRY OF THE KORNERUPINE–PRISMATINE SERIES. I. CRYSTAL STRUCTURE AND SITE POPULATIONS

MARK A. COOPER AND FRANK C. HAWTHORNE§

Department of Geological Sciences, University of Manitoba, Winnipeg, Manitoba R3T 2N2, Canada

EDWARD S. GREW

Department of Earth Sciences, University of Maine, Orono, Maine 04469, U.S.A.

ABSTRACT

The crystal structures of forty-seven crystals of the kornerupine–prismatine series have been refined to *R* indices of 1.6–2.5% using single-crystal X-ray data. Samples were selected to cover as wide a range of chemical composition as possible. The principal crystal-chemical problems (Si, Al and B distributed over three *T* sites, Mg, Al, Fe^{2+}, Fe^{3+} and □ distributed over five *M* sites and one *X* site, and variable H in the structure) required the development of a new approach to site-population assignment. This approach involved (1) a relatively large number of crystals covering the entire compositional range of kornerupine–prismatine, (2) a synergy among site-scattering refinement, electron-microprobe analysis and the development of mean-bond-length – constituent-cation radius relations at all sites in the structure for all forty-seven crystals simultaneously, until self-consistency was achieved for the entire dataset. Crystals of the kornerupine–prismatine series are orthorhombic, space group *Cmcm*, *a* 15.92–16.13, *b* 13.66–13.76, *c* 6.69–6.76 Å, (□,Mg,Fe) $(Al,Mg,Fe)_9$ $(Si,Al,B)_5$ O_{21} (OH,F), $Z = 4$. Boron is completely ordered at the *T*(3) site, whereas Si and Al occur at all three *T* sites, with Si >> Al at *T*(1), Si ≥ Al at *T*(2) and Si ≥ Al at *T*(3). The *M* sites are occupied as follows: *M*(1) by Mg and Fe^{2+}, with Mg > Fe^{2+}, *M*(2) by Mg, Fe^{2+} and Al, with (Mg ≥ Fe^{2+}) > Al, *M*(3) by Al and Mg, with Al >> Mg, *M*(4) by Al, Mg, Fe^{3+} and minor amounts of Ti, Cr^{3+} and V^{3+}, with Al > Mg > Fe^{3+}, *M*(5) by Al and Mg, with Al >> Mg. The *X* site is occupied by □ (vacancy), Mg, Fe^{2+} and minor Na and Ca, with □ > Mg ≈ Fe^{2+}.

Keywords: kornerupine–prismatine, crystal-structure refinement, electron-microprobe analysis, site-populations, order–disorder.

SOMMAIRE

Nous avons résolu la structure cristalline de quarante-sept cristaux, membres de la série kornérupine–prismatine, jusqu'à un résidu *R* entre 1.6 et 2.5% au moyen de données en diffraction X obtenues sur monocristaux. Nous avons choisi les échantillons pour représenter la série aussi complètement que possible. Les principaux défis cristallochimiques auxquels nous avons fait face (Si, Al etd B distribués sur trois sites *T*, Mg, Al, Fe^{2+}, Fe^{3+} et □ distribués sur cinq sites *M* et un site *X*, et une teneur variable en H dans la structure) imposent une nouvelle approche pour répartir les atomes parmi ces sites. Ainsi, cette nouvelle façon de faire a impliqué (1) un nombre relativement élevé de cristaux représentatifs de la série kornérupine–prismatine, (2) une synergie parmi les affinements de la dispersion des électrons aux sites cités, les résultats d'analyses par microsonde électronique, et le

§ *E-mail address*: frank_hawthorne@umanitoba.ca

développement de relations entre longueur de liaison moyenne et rayon des cations présents à ces sites, ceci pour tous les sites dans la structure des 47 cristaux simutanément, jusqu'à cohérence interne pour le jeu de données au complet. Les cristaux de la série kornérupine–prismatine ont une symétrie orthorhombique, groupe spatial *Cmcm*, *a* 15.92–16.13, *b* 13.66–13.76, *c* 6.69–6.76 Å, ($\square$,Mg,Fe) (Al,Mg,Fe)$_9$ (Si,Al,B)$_5$ O$_{21}$ (OH,F), $Z = 4$. Le bore est complètement ordonné au site *T*(3), tandis que Si et Al occupent les trois sites *T*, avec Si >> Al à *T*(1), Si ≥ Al à *T*(2), et Si ≥ Al à *T*(3). Les sites *M* sont remplis comme suit: *M*(1) par Mg et Fe^{2+}, avec Mg > Fe^{2+}, *M*(2) par Mg, Fe^{2+} et Al, avec (Mg ≥ Fe^{2+}) > Al, *M*(3) par Al et Mg, avec Al >> Mg, *M*(4) par Al, Mg, Fe^{3+} et de faibles quantités de Ti, Cr^{3+} et V^{3+}, avec Al > Mg > Fe^{3+}, et *M*(5) par Al et Mg, avec Al >> Mg. Le site *X* contient $\square$ (lacune), Mg, Fe^{2+} et une quantité moindre de Na et Ca, avec $\square$ > Mg ≈ Fe^{2+}.

Mots-clés: kornérupine–prismatine, affinement de la structure cristalline, données de microsonde électronique, occupation des sites, ordre–désordre.

Introduction

Kornerupine *sensu stricto* and prismatine, B-poor and B-rich members of the kornerupine series (Grew *et al.* 1996, Braga *et al.* 2003), have been reported from some 70 localities worldwide. With rare exceptions, they occur in Precambrian upper-amphibolite- and granulite-facies terranes, and most estimates of their conditions of formation lie in the ranges 700 < T < 1000°C and 4.0 < P < 12.5 kbar (Grew 1996). Kornerupine *sensu lato* is orthorhombic, space group *Cmcm*, and Grew (1996) gave the general formula as $^{[8]}(\square,Fe,Mg)\ ^{[6]}(Al,Mg,Fe)_9\ ^{[4]}(Si,Al,B)_5\ (O,OH,F)_{22}$. This formula does not seem unduly complicated, but the combination of variable amounts of light elements (H, B) and vacancies ($\square$) and numerous sites occupied by similar cations in the structure (three tetrahedrally coordinated sites and five octahedrally coordinated sites) greatly hinders the assignment of accurate site-populations. The problem is further complicated by the fact that Fe occurs as both Fe^{2+} and Fe^{3+}, and that the Mössbauer spectra of Fe-bearing species are difficult to fit (Grew *et al.* 1999). Moreover, the response of the structure to compositional variations is quite subtle, and it is difficult to convincingly derive site populations by crystal-structure refinement and absorption spectroscopy. This problem may be ameliorated by examining a relatively large number of crystals spanning the complete range of chemical variation, as done with staurolite (*e.g.*, Hawthorne *et al.* 1993a, b, c). In this series of papers, we use this philosophy to further understand the crystal chemistry of kornerupine. Here, we denote kornerupine *sensu lato* as kornerupine, and kornerupine *sensu stricto* as kornerupine(*ss*).

Previous Work

There has been considerable structural and chemical work on kornerupine (Grew 1996); the salient features are briefly reviewed here.

Crystal structure

The crystal structure of kornerupine was solved by Moore & Bennett (1968) on a crystal from Mautia Hill, Tanzania. Further refinements were presented by Moore & Araki (1979; synthetic crystal with 2.73 wt.% B_2O_3), Finger & Hazen (1981; crystal stated to be from Rangeley Quadrangle, Maine, but actually from Gananoque, Ontario, Grew 1996), Moore *et al.* (1989; Mautia Hill, Tanzania), and Klaska & Grew (1991; crystal from the Limpopo Belt, Zimbabwe).

The structure of kornerupine (Moore & Araki 1979) is a complex densely organized arrangement comprised of two kinds of layers oriented parallel to (010). The A layer (Fig. 1) is based on walls of edge-sharing and corner-sharing octahedra. These walls are four octahedra wide along [100], extend parallel to [001], and link together along [100] through edge-sharing distorted cubes that contain the *X* cation. All of the cation sites within the A layer [*X*, *M*(3), *M*(5)] have fractional coordinates $y = z = 0$ and are symmetrically constrained to lie on the *c* glide-plane at $y = 0$.

Sandwiching the A layer is the B layer (Fig. 2), consisting of *M*(1), *M*(2), *M*(4) octahedra and *T*(1), *T*(2) and *T*(3) tetrahedra. The octahedra link to form chains along [100] by edge-sharing in the sequence = *M*(1) = *M*(4) = *M*(2) = *M*(4) = *M*(1) =, and by corner-sharing between *M*(1) octahedra. The chains of octahedra are linked in the [001] direction *via* corner-sharing with [T_2O_7], *T*(1)–*T*(1), and [T_3O_{10}], *T*(2)–*T*(3)–*T*(2), units which alternate along [100].

The linkage between the A and B layers is shown in Figure 3. The octahedra of both layers nestle neatly together to form a compact edge-sharing cluster. The *n*-glide parallel to (010) at $y = (¼, ¾)$ relates two B layers (B and B') that link by edge-sharing between *M*(1) octahedra of the B layer and *T*(2) tetrahedra of the B. layer, and by corner-sharing between *M*(4) octahedra of the B layer and *T*(1) tetrahedra of the B' layer. The structure repeats along [010] in the fashion *...ABBABBA...* .

Site occupancy

Moore & Bennett (1968) assigned Mg to two of the five octahedrally coordinated sites, and Al to the remaining three octahedrally coordinated sites. Hydroxyl was assigned to the O(10) anion site. The B content (1.92 wt.% B_2O_3, McKie 1965) of this sample

was not assigned to any of the tetrahedrally coordinated sites; however, it is apparent from inspection of the isotropic-displacement parameters that B resides at the tetrahedrally coordinated site labeled *Si*(2) [later named the *T*(3) site by Moore & Araki 1979]. The magnitude of the displacement parameter for the atoms at the *Si*(2) position is more than twice that at the other two tetrahedrally coordinated sites; this observation is consistent with significant substitution of an element appreciably lighter than Si (*i.e.*, B) at the *Si*(2) site.

Moore & Araki (1979) refined the structure of a synthetic kornerupine containing 2.73 wt.% B_2O_3 (Werding & Schreyer 1978). This synthetic sample is devoid of Fe and provided an opportunity to study the structural sites with one fewer chemical variable present. Moore & Araki (1979) concluded that (1) all B resides at *T*(3), (2) a partly occupied eight-coordinated cation-site, *X*, occurs at the origin and contains ($Mg_{1/3} + \square_{2/3}$), and (3) the O(10) site contains an OH group, providing one (OH) per 22 anions. Comparison of various data on kornerupine led them to postulate that the O(10) position could vary in composition from $(O^{2-})_1$ $(OH)_0$ to $(O^{2-})_0(OH)_1$ and that this variation couples to an *X* occupancy variable from 1 to ⅓, respectively. Finger & Hazen (1981) clearly demonstrated that Fe is ordered at two of the octahedrally coordinated sites [*M*(1) and *M*(2)] by refinement of a sample of Fe-rich kornerupine (12.2 wt.% FeO, 3.09 wt.% B_2O_3). They suggested that there are no obvious structural limitations on the degree of Fe ⇌ Mg substitution.

Moore *et al.* (1989) gave evidence for Fe^{3+} at the *M*(4) site. They revised their inferences about the O(10) site to include compositions from $(O^{2-})_1(OH)_0$ to $(O^{2-})_{1/3}(OH)_{2/3}$ with a coupled *X* occupancy from 1 to ⅓, respectively. Klaska & Grew (1991) refined the structure of B-free kornerupine and concluded that low-B kornerupine probably has Al at *T*(3). Comparison of the earlier structural studies [Finger & Hazen (1981): B = 0.69 *apfu*; Moore & Araki (1979): B = 0.58 *apfu*; Moore *et al.* (1989): B = 0.41 *apfu*] with their study (B = 0 *apfu*) led them to suggest a coupled substitution of B for Si and Al at *T*(3) and Si for Al at *T*(2), together with complex substitutions at the octahedrally coordinated sites. A disordered H-position was located, and an interpretation for both OH and H_2O at O(10) was given. The O(10) site contains both OH and F, and a discussion involving further substitution by H_2O suggested the possibility of more than 1 H *apfu*.

In Table 1, we summarize the individual results, as well as the inferred schemes of order for the data presented in those studies.

Experimental Methods

Samples

Forty-seven samples were used in this work. We tried to cover the entire observed compositional range of kornerupine–prismatine; specific analyzed samples were obtained from authors of various published studies to ensure this coverage. Small amounts of Li and Be have been reported in kornerupine (Grew 1996); these constituents are not considered here, although Cooper *et al.* (2009b) do characterize the degree of order of Be in Be-rich kornerupine. The provenance of the samples is indicated in Table 2.

Collection of X-ray data

Crystals of kornerupine commonly contain microfractures, altered margins and a wide variety of inclusions. Equidimensional fragments (0.2–0.3 mm) were examined under normal, plane-polarized and cross-polarized light to ensure freedom from cracks, uniform color, high optical clarity and freedom from inclusions. Suitable fragments were abraded to a spherical or elipsoidal shape in a Nonius air grinder in order to minimize anisotropic X-ray absorption.

Crystals were then mounted on a Siemens *P*3 single-crystal diffractometer equipped with graphite-monochromated Mo*K*α X-radiation. The crystals were optically aligned within the X-ray beam, and 25 reflections from a rotation photo were centered. The cell parameters (Table 3) and orientation matrix were derived by least-squares refinement of the setting angles of the centered reflections. Crystal quality was assessed at this stage *via* the profiles of Bragg diffraction peaks and cell-parameter standard deviations, with rejection of unsuitable candidates. A single asymmetric unit of intensity data was collected ($4 \rightarrow 60°$ 2θ; $0 \le h \le 22$, $0 \le k \le 19$, $0 \le l \le 9$; θ–2θ scan mode, 96 steps per reflection; 2.2° 2θ scan range, $4 \rightarrow 30°$ 2θ/min. variable scan-rate). Two standard reflections were collected every 50 measurements to monitor instrument stability. After the intensity dataset was collected, a psi-scan data set was collected so that an empirical absorption-correction could be applied. It consisted of eleven strong reflections uniformly distributed with regard to 2θ and measured over 10° intervals of Ψ (the azimuthal angle corresponding to rotation of the crystal about its

TABLE 1. SCHEMES OF ORDER IN KORNERUPINE USED PREVIOUSLY

Site	Moore & Araki (1979) B = 0.58 *apfu*	Finger & Hazen (1981) B = 0.69 *apfu*	Moore *et al.* (1989) B = 0.41 *apfu*	Klaska & Grew (1991) B = 0 *apfu*
X	□,Mg,Fe,(Na,Ca)	□,Mg,Fe	□,Mg	□,Mg,Fe
M(1)	Mg,Fe	Mg,Fe	Mg	Mg,Fe
M(2)	Mg	Mg,Fe	Mg,Al	Mg
M(3)	Al	Al	Al,Mg	Al
M(4)	Al,Mg,Fe^{3+},(Ti,Cr^{3+})	Al,Fe^{3+},Mg	Al,Mg,Fe^{3+}	Al,Mg
M(5)	Al	Al	Al	Al
T(1)	Si	Si	Si	Si
T(2)	Si,Al	Si,Al	Si,Al	Al,Si
T(3)	B,Si	B,Si	Si,B	Si,Al
O(10)	OH^-	OH^-	O^{2-},OH^-	OH^-,F^-,(H_2O?)

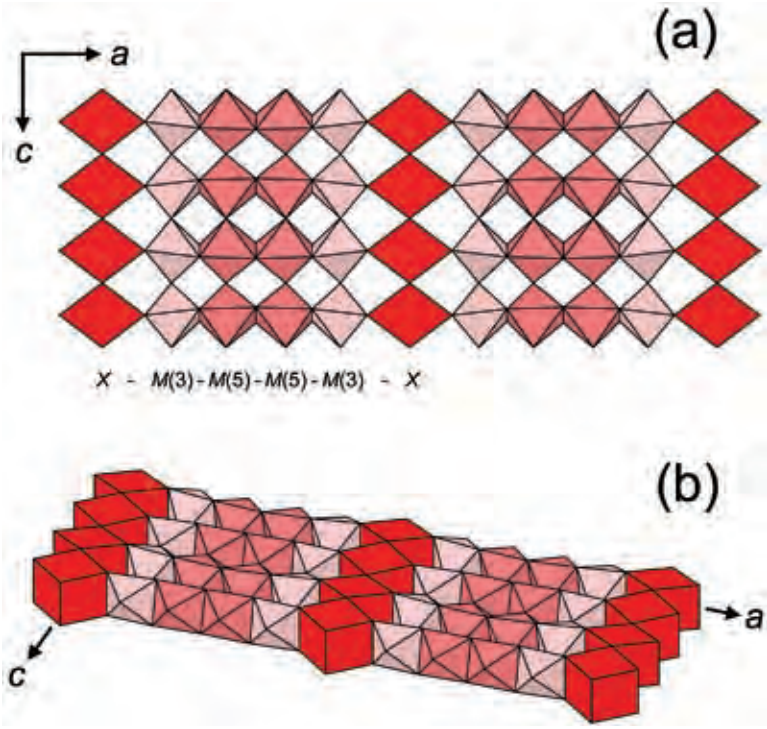

FIG. 1. The structure of kornerupine: (a) the A layer projected down [010]; (b) perspective view of the A layer.

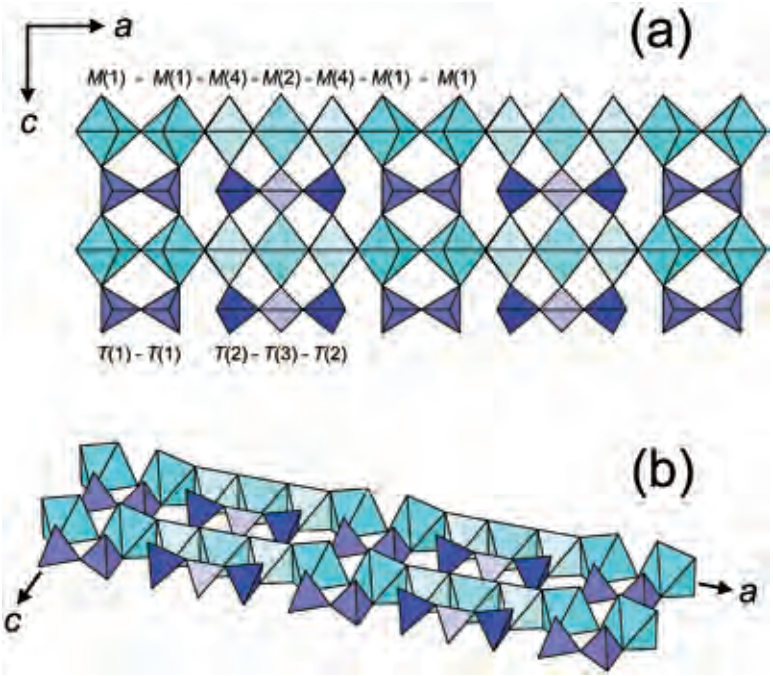

FIG. 2. The crystal structure of kornerupine: (a) the B layer projected down [010]; (b) perspective view of the B layer.

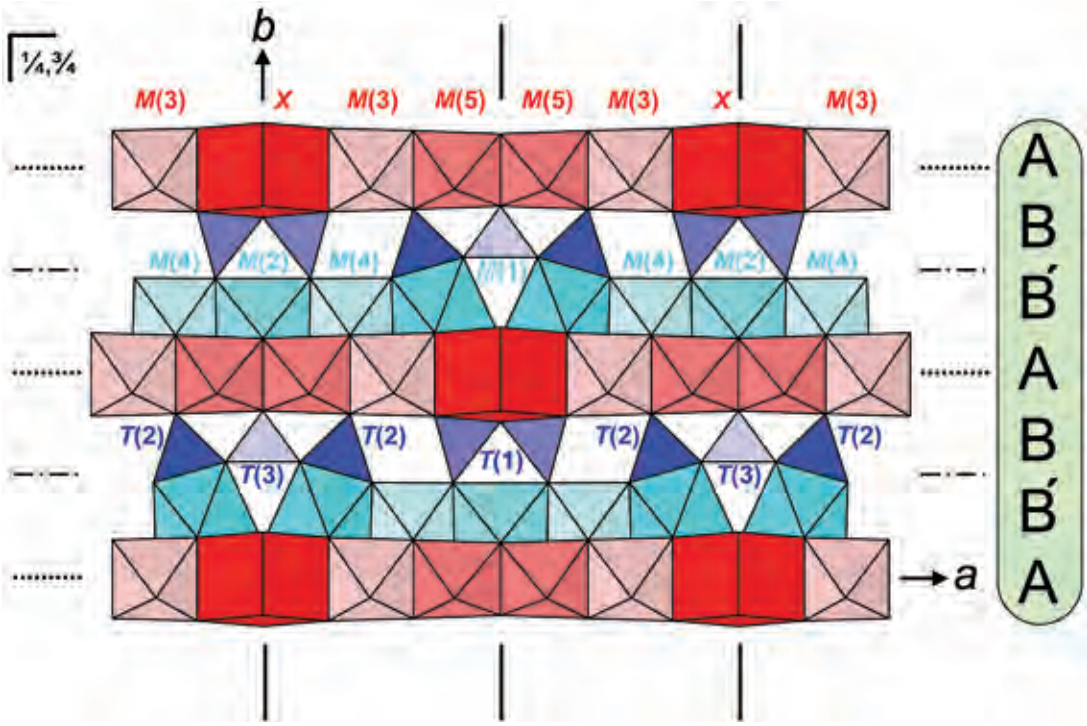

FIG. 3. The kornerupine structure projected down [001]; A-layer components are shown in red hues and reside on the *c*-glide plane (010) at $y = 0,½$; B-layer components are shown in blue hues and relate to each other across the *n*-glide plane (010) at $y = ¼,¾$. Along the *c* axis (perpendicular to the page), A-layer components are at $z = 0,½$; B-layer components are on the mirrors (001) at $z = ¼, ¾$. The *C*-centered cell is marked by the *X* sites.

diffraction vector) from 0 to 360° Ψ. After absorption corrections, $<R_{azimuthal}>$ values were ≤1.3%.

The Siemens SHELXTL (PC version) system of programs was used throughout this study. Data reduction included scaling on the standard reflections and applying standard drift, Lorentz, polarization and background corrections. These data were then corrected for absorption using the Ψ-scan data, with the crystal modeled as an ellipsoid. The resulting data were reduced to structure factors, resulting in ~1200 reflections with ~1050 with $|F_o| > 4\sigma F$ that were used for full-matrix least-squares refinement of the structure.

Electron-microprobe analysis (EMPA)

After the intensity-data collection, the crystals were fixed to 2.5-cm plexiglass disks with a thermal-setting epoxy (PETROPOXY™), and the surface was polished and carbon-coated. Electron-microprobe analysis was done on a CAMECA SX–50 instrument using back-scattered electron (BSE) imaging and energy-dispersion spectrometry (EDS) for qualitative assessment, and wavelength-dispersion spectrometry (WDS) for the acquisition of quantitative chemical compositions. All crystals were initially prescreened using BSE imaging to check for element zonation; none was detected for any crystal. Next, an ED spectrum was collected for each crystal in order to identify all X-ray emission lines and thereby ensure complete coverage of elements during subsequent WDS analysis. The following standards and spectrometer crystals were used for *K*α spectral lines: Si, diopside, PET; Al, kyanite, TAP; Mg, forsterite, TAP; Fe, fayalite, LiF; Na, albite, TAP; Mn, spessartine, LiF; V, VP_2O_7, LiF; Ti, titanite, LiF; Ca, diopside, PET; K, orthoclase, PET (not detected); Cr, chromite, PET; F, fluororiebeckite, TAP. Analyses in the WDS mode were done with the following operating conditions: 15 kV excitation voltage; 20 nA sample current; 20 s peak count time; 10 s background count time. Ten random points were analyzed per crystal using a beam diameter of 2 μm. Data reduction was done with the φ(ρZ) method (Pouchou & Pichoir 1984, 1985), and average compositions are given in Table 4.

Calculation of the Unit Formula

This is a very non-trivial calculation, as values for the B_2O_3 content are essential, and the behavior of H in the structure (or analyzed values for H_2O) needs to be known. The crystal-structure refinement procedure derived accurate B_2O_3 values, and thus there was a synergic interaction between calculation of the unit formula and the structure-refinement process. The situation for Fe_2O_3 was similar. Final formulae were obtained only at the end of the refinement process. Initially, we assumed (OH + F) = 1.0 *apfu* and calculated the formulae accordingly, despite several proposals to the contrary (Table 1); detailed analytical and spectroscopic work finally showed this assumption to be correct (Cooper *et al.* 2009a). Final unit formulae are given in Table 4.

Crystal-Structure Refinement

The structure was refined on F^2 using neutral scattering factors for cations, absorption coefficients and anomalous dispersion corrections from the International Tables for Crystallography (1992) for all cations. Scattering factors for ionized species were used for oxygen [O^{2-}] (Azavant & Lichanot 1993) and fluorine [F^-] (International Tables for Crystallography 1992). The use of this combination of scattering factors is justified in Appendix 1. The expressions for *R* indices, weighting factors, extinction coefficients and atom-displacements models are given in Appendix 2.

Derivation of complete site-populations and chemical formulae requires information from both the structure refinement *and* the formulae calculated from the electron-microprobe data. However, the formulae cannot be calculated without data from the crystal-structure refinements, and the crystal-structure refinements cannot be done correctly without information from the formulae. Thus crystal-structure refinement and formula calculation must be done iteratively until self-consistency of all results is achieved. Furthermore, the procedure had to be applied *simultaneously* to *all forty-seven structures examined* in order to understand the significance of some of the more subtle changes, a process we call *iterative batch-refinement.* There were three principal steps in the refinement, *primary*, *secondary*, and *tertiary*; the scattering species assigned to each site are shown in Table 5, and the formula-

TABLE 2. KORNERUPINE: SAMPLE NUMBERS AND CODES, LOCALITIES AND REFERENCES

This study	Locality	Ref.	Other number	Source	This study	Locality	Ref.	Other number	Source
K1	Ellammankovilpatti, India	(1)	3083D	(a)	K26	Labwor Hills, Uganda	(1)	PHN984	(f)
K2	Bjørnesund, W.Greenland	(8)	133771	(b)	K27	Namaqualand, S.Africa	(6)	DWN138	(o)
K3	Kondapalle, Andhra Pradesh, India	(1)	J-21	(c)	K28	Madagascar	(1)	BM1972,170	(d)
K5	Elahera, Sri Lanka	(8)	—	(i)	K29	Aldan Shield, Yakutia, Russia	(5)	142-1C	(a)
K6	Aldan Shield, Yakutia, Russia	(5)	134E	(a)	K30	Darai Stazh, SW Pamirs, Tajikistan	(7)	DC707H	(q)
K7	Madagascar	(1)	171.350	(k)	K31	Darai Stazh, SW Pamirs, Tajikistan	(7)	DC9141B	(r)
K8	Ponakkadu, India	(1)	3053B	(a)	K32	Sri Lanka	(8)	—	(j)
K9	Madagascar	(1)	141255	(b)	K33	Paderu, Andhra Pradesh, India	(1)	E2724	(g)
K10	Lac Ste-Marie, Quebec, Canada	(8)	24518	(e)	K34	Waldheim, Germany	(2)	1892.1438	(h)
K11	Port Shepstone, S.Africa	(1)	BM1940,39	(d)	K35	Sinyoni Claims, Limpopo, Zimbabwe	(1)	9365	(p)
K12	Fiskenæsset, Greenland	(2)	31498	(e)	K36	Reynolds Range, Australia	(3)	XF-4	(s)
K13	Aldan Shield, Yakutia, Russia	(5)	134H	(a)	K38	Walton's locality, Fiskenæsset, Greenland	(10)	—	(h)
K14	Wright locality, Lac Ste-Marie, Quebec	(8)	5410	(a)	K39	Walton's locality, Fiskenæsset, Greenland	(10)	—	(h)
K15	Baldwin Locality, Harts Range, Australia	(8)	5032	(m)	K40	Walton's locality, Fiskenæsset, Greenland	(10)	—	(h)
K16	Lac Ste-Marie, Quebec, Canada	(8)	5400C	(a)	K41	near Itrongahy, Madagascar	(1)	112233	(i)
K17	Harts Range, Australia	(8)	24752	(n)	K42	Reading Prong, New Jersey, USA	(4)	T-8	(t)
K18	Namaqualand, S.Africa	(6)	K2-F	(o)	K43	Tanzania	(8)	—	(j)
K19	Waldheim, Germany	(2)	5126AA	(a)	K45	Sri Lanka	—	1774	(v)
K20	Waldheim, Germany	(2)	12567	(e)	K46	Mindi Hills, Kenya	(8)	729	(v)
K21	Ellammankovilpatti, India	(1)	3083E2	(a)	K47	Mindi Hills, Kenya	(8)	729	(v)
K22	Sinyoni Claims, Limpopo, Zimbabwe	(8)	8497	(p)	K49	Madagascar	(8)	263	(v)
K23	Kwale, Kenya	(8)	BM1978,467	(d)	K50	Sinyoni Claims, Limpopo, Zimbabwe	(8)	1577	(v)
K24	Waldheim, Germany	(2)	5105M	(a)	K52	Stakholmen, Hälsingland, Sweden	(9)	—	(u)
K25	Larsemann Hills, East Antarctica	(8)	8812903	(q)					

Museum number or collection of: (a) Ed Grew; (b) National Museum of Natural History, Smithsonian Institution; (c) J.K. Nanda; (d) Natural History Museum, London; (e) American Museum of Natural History; (f) P.H. Nixon; (g) Royal Ontario Museum; (h) Geologisk Museum (Copenhagen); (i) Harvard University Mineralogical Museum; (j) purchased from dealer; (k) Muséum National d'Histoire Naturelle, Paris; (l) Juergen Malley; (m) R.G. Warren; (n) Adelaide University; (o) D.J. Waters; (p) Institut für Mineralogie, Ruhr-Universität Bochum; (q) Douglas E. Thost; (r) N.N. Pertsev; (s) Julie K. Vry; (t) D. Young; (u) Erik Jonsson; (v) (K45, originally obtained from R. Holland; K46, K47, originally obtained from Campbell Bridges; K49, originally obtained from Ed Swoboda; K50, Rossman number 1577, originally 8497 from Ruhr-Universität, Bochum) George Rossman, Ed Swoboda.

References: (1) Schreyer & Abraham (1976), Nixon *et al.* (1984), Grew *et al.* (1990a, and references cited therein), Klaska & Grew (1991); (2) Grew *et al.* (1987, 1996); (3) Vry (1994), Vry & Cartwright (1994); (4) Young (1995); (5) Grew *et al.* (1991a,b); (6) Waters & Moore (1985); (7) Grew *et al.* (1990b, 1998); (8) Grew *et al.* (1990a, and references cited therein); (9) Jonsson (1996); (10) Petersen & Secher (1993).

normalization procedure is shown in Figure 4. This procedure is intended to derive accurate values for the B and Fe^{3+} contents of all kornerupine crystals. It must be emphasized that this procedure, complicated as it is, was essential to the resolution of the compositional and structural problems of kornerupine. As the general approach used here is rather different from that used normally for crystal-structure refinement, it is described in some detail.

As the iterative refinement procedure uses stereochemical details to guide the process of refinement, particularly with regard to dealing with site occupancies, we list the final data of the refinement here. All final coordinates and anisotropic-displacement factors of the atoms may be obtained from the Depository of Unpublished Data on the MAC website [document Kornerupine CM47_233]. Selected interatomic distances, refined site-scattering values and site populations are given in Tables 6 and 7.

TABLE 3. INFORMATION CONCERNING X-RAY DATA COLLECTION AND STRUCTURE REFINEMENT

	Cell parameters				R_1 ($\|F_o\| > 4\sigma$) %	wR_2 (F_o^2) %
	a (Å)	*b* (Å)	*c* (Å)	*V* (Å^3)		
K1	16.036(3)	13.710(2)	6.723(1)	1478.2(4)	1.7	4.6
K2	16.014(4)	13.728(2)	6.710(1)	1475.1(5)	1.9	4.9
K3	15.956(3)	13.689(3)	6.695(1)	1462.4(5)	1.9	4.9
K5	15.940(3)	13.701(2)	6.694(1)	1461.9(4)	2.0	5.1
K6	15.970(6)	13.721(3)	6.712(2)	1470.7(7)	2.0	5.2
K7	15.943(3)	13.716(2)	6.692(1)	1478.2(4)	1.9	5.2
K8	16.007(4)	13.749(3)	6.725(1)	1475.1(5)	2.3	5.6
K9	15.926(4)	13.704(4)	6.695(2)	1461.4(6)	2.0	5.1
K10	15.972(5)	13.728(3)	6.708(2)	1470.8(7)	1.9	5.1
K11	15.946(4)	13.679(3)	6.693(2)	1459.9(6)	1.8	4.9
K12	16.050(6)	13.742(4)	6.728(2)	1483.7(7)	2.1	5.1
K13	15.929(4)	13.718(4)	6.688(2)	1461.5(7)	2.0	5.3
K14	15.968(8)	13.704(4)	6.708(2)	1467.9(9)	1.7	5.0
K15	16.007(5)	13.746(4)	6.708(3)	1475.9(9)	1.9	5.6
K16	15.931(5)	13.660(5)	6.699(2)	1457.8(8)	1.8	4.7
K17	15.987(5)	13.740(3)	6.702(2)	1472.2(7)	1.9	5.4
K18	15.970(2)	13.720(2)	6.703(1)	1475.1(5)	1.9	5.4
K19	15.938(2)	13.670(3)	6.690(1)	1457.6(4)	1.8	4.8
K20	15.938(3)	13.673(3)	6.693(1)	1470.8(7)	1.9	5.1
K21	16.061(3)	13.718(2)	6.729(1)	1482.7(4)	2.1	6.4
K22	16.031(3)	13.704(2)	6.714(1)	1475.1(4)	1.9	5.0
K23	15.943(2)	13.701(2)	6.693(1)	1462.1(3)	1.7	5.0
K24	15.949(2)	13.669(2)	6.692(1)	1459.0(4)	2.1	5.5
K25	15.953(3)	13.723(2)	6.700(1)	1466.8(4)	1.9	5.3
K26	16.025(3)	13.742(2)	6.722(1)	1480.2(4)	2.4	6.3
K27	15.960(2)	13.725(2)	6.705(1)	1468.7(3)	2.1	5.4
K28	15.943(3)	13.725(1)	6.699(1)	1465.9(3)	2.2	5.3
K29	15.976(2)	13.710(2)	6.710(1)	1469.6(3)	2.2	6.7
K30	16.111(2)	13.708(2)	6.733(1)	1487.0(4)	2.1	6.1
K31	16.025(5)	13.703(3)	6.721(2)	1475.9(6)	2.5	7.0
K32	15.942(2)	13.708(2)	6.693(1)	1462.8(4)	2.0	5.3
K33	16.003(2)	13.702(3)	6.709(1)	1471.1(4)	1.9	5.1
K34	15.980(3)	13.697(2)	6.696(2)	1465.5(5)	2.0	5.4
K35	16.130(3)	13.744(3)	6.758(2)	1498.1(6)	2.0	5.2
K36	16.125(2)	13.761(2)	6.758(1)	1499.4(3)	1.8	4.8
K38	16.071(2)	13.746(2)	6.736(1)	1487.9(4)	1.7	4.6
K39	16.036(3)	13.732(2)	6.720(1)	1479.7(4)	1.8	5.2
K40	16.118(2)	13.732(2)	6.755(1)	1494.9(3)	1.6	4.6
K41	15.919(1)	13.727(1)	6.692(1)	1462.4(2)	2.1	5.9
K42	15.941(1)	13.696(1)	6.697(1)	1462.2(2)	2.2	5.3
K43	15.965(2)	13.697(1)	6.701(1)	1465.2(2)	1.9	5.2
K45	15.941(2)	13.696(2)	6.692(1)	1461.2(3)	2.5	6.6
K46	16.056(2)	13.717(2)	6.720(1)	1480.0(3)	2.1	5.6
K47	16.050(1)	13.715(1)	6.720(1)	1479.3(2)	2.1	5.6
K49	15.955(1)	13.721(1)	6.701(1)	1466.8(2)	2.4	6.2
K50	16.053(2)	13.702(1)	6.717(1)	1477.4(3)	2.3	5.8
K52	15.992(2)	13.721(2)	6.705(1)	1471.2(3)	2.1	5.5

Primary refinement

As a first approximation, B is assumed to be fully ordered at the *T*(3) site (*cf.* Klaska & Grew 1991); the *T*(3) site is thus occupied by B, Si and Al. Three site occupancies cannot be resolved at a site using diffraction data only. However, the relative scattering-factors of these three species scale as their atomic numbers: B = 5, Al = 13, Si = 14. Hence Si and Al can be combined (and expressed as Si, the dominant constituent), and the relative occupancies of Si (+ Al) and B can be derived by site-scattering refinement.

The Fe^{3+} content was initially considered to be fully ordered at the *M*(4) site, with all Fe at *M*(4) in the ferric state: *M*(4) = Fe^{3+}, Mg, Al. The X-ray scattering by these species scales as their atomic numbers: Mg = 12, Al = 13, Fe = 26. Hence Mg and Al can be combined (and expressed as Al, the dominant constituent) and the relative occupancies of Al (+ Mg) and Fe (≡ Fe^{3+}) can be derived by site-scattering refinement.

The results of the primary stage of refinement provide preliminary contents of B and Fe^{3+} for each crystal, and these values can be used in the initial calculation of the formulae from the electron-microprobe data.

Secondary refinement

In order to improve the B value from the primary refinement of the structure, the Al content at *T*(3) needs to be derived and then modeled in the refinement by incorporating the Al scattering factor at *T*(3). Moreover, the other *T* sites need to be modeled in terms of Si–Al distribution so that the overall refinement is better scaled. The Al content at *T*(3) can be derived as follows:

(1) From the results of the initial refinement, approximate values of B and Fe^{3+} are used to process the EMP data and provide the number of Si cations *apfu*;

(2) All Si resides at the three *T* sites. As the total Si and B *apfu* are known, the Al content of the *T* sites can be calculated by difference: $^{[4]}$Al = 5 – Si – B;

(3) The three occupants in question (B, Si, Al) have quite different radii (0.11; 0.26; 0.39 Å, respectively; Shannon 1976). Occupancy by these cations is thus recorded in the bond-length information. From the amounts of ($^{[4]}$Si, $^{[4]}$Al, $^{T(3)}$B) and the <*T*–O> bond-lengths, the Si and Al populations for all *T* sites can be calculated.

Point (3) requires some assumptions concerning the *T*(1) site: (1) The shortest <*T*(1)–O> distance observed in this study (1.618 Å, Table 6) corresponds to complete occupancy of the *T*(1) site by Si. (2) Replacement of Si by Al conforms to a hard-sphere model. These two assumptions define a relation between <*T*(1)–O> and constituent-cation radius [<*T*(1)–O> = (1.618–0.26) + 1.0 $<r^{T(1)}>$] such that Si and Al site-populations can be calculated for all forty-seven crystals.

The <*T*(2)–O> distances observed here (Table 6) are in the range 1.646–1.698 Å; clearly there is significant variation in Si and Al at this site. The range of distances indicates that *all* crystals contain significant Al at *T*(2), and hence we cannot derive an equation in the same way as was done for the *T*(1) site. The situation at the *T*(3) site is even more complicated, with variable occupancy by Si, Al and B; the site populations of Si and Al at *T*(2) and *T*(3) were derived in the following manner:

(1) For a <*T*(2)–O> *versus* constituent-cation radius relation, minimum values for the intercept and slope were chosen.

(2) For this set of intercept and slope values, the $^{T(2)}$Si and $^{T(2)}$Al site-occupancies were calculated.

(3) $^{T(3)}$Si is calculated from the relation $^{T(3)}$Si = ^{EMP}Si – $^{T(1)}$Si – $^{T(2)}$Si.

(4) $^{T(3)}$Al is calculated from the relation $^{T(3)}$Al = 1.0 – $^{T(3)}$Si – $^{T(3)}$B.

(5) The resulting relation between <*T*(3)–O> and the constituent-cation radius at the *T*(3) site was evaluated by linear regression (and visual inspection).

(6) Values of the slope and intercept for the *T*(2) site [see step(1)] were incremented, and steps (1) → (5) were repeated over physically reasonable ranges of <*T*(2)–O> and <$r^{T(2)}$>.

(7) The best fit for the *T*(3) site, as assessed *via* the correlation coefficients produced from step (5), defined the optimum values of the intercept and slope for the <*T*(2)–O> *versus* <$r^{T(2)}$> relation, and produced site populations for all *T* sites.

(8) The resulting values of $^{T(1)}$Si, $^{T(1)}$Al, $^{T(2)}$Si, $^{T(2)}$Al and $^{T(3)}$Al were considered as fixed in the next series

TABLE 4. KORNERUPINE: CHEMICAL COMPOSITIONS (wt %) AND UNIT FORMULAE (*apfu*)

	K1	K2	K3	K5	K6	K7	K8	K9	K10	K11	K12	K13	K14	K15	K16	K17
SiO_2	29.97	30.75	29.30	30.82	29.60	31.63	29.01	30.89	29.96	29.10	29.78	32.38	29.98	29.69	29.70	29.86
Al_2O_3	44.06	42.98	41.45	42.21	40.40	40.56	41.36	40.11	40.36	41.35	45.72	40.50	40.73	37.75	40.98	38.57
B_2O_3*	1.88	2.41	3.76	3.52	3.37	3.56	2.51	3.96	3.22	3.89	1.39	4.08	3.47	3.24	3.93	3.52
MgO	17.32	18.79	12.84	17.21	14.27	19.20	15.03	18.05	15.15	10.81	19.45	21.20	18.83	16.03	11.97	15.24
FeO	3.80	2.25	9.01	4.09	8.20	2.83	7.41	4.26	7.62	12.09	1.08	0.76	8.07	7.25	10.31	7.34
Fe_2O_3**	0.73	0.86	1.51	0.04	1.81	0.52	2.21	0.60	1.52	–	0.34	0.09	1.69	3.63	0.59	3.44
MnO	–	–	–	0.13	0.35	–	0.31	0.13	–	0.12	–	–	–	–	–	–
V_2O_3	–	–	–	–	–	–	–	–	–	–	–	–	–	–	–	–
Cr_2O_3	–	–	–	–	–	–	–	–	–	–	–	–	–	–	–	–
TiO_2	0.12	–	–	–	–	–	–	–	0.13	0.21	–	–	0.13	0.15	0.19	–
Na_2O	0.04	–	0.10	0.04	0.04	–	–	0.05	–	0.05	–	–	–	0.11	–	0.12
CaO	–	–	–	–	–	–	–	–	–	–	0.08	–	–	–	–	–
F	0.07	0.04	0.74	0.43	0.46	0.30	0.02	0.38	0.11	0.85	0.03	0.18	0.17	0.49	0.39	0.37
H_2O***	1.17	1.20	0.84	1.01	0.97	1.08	1.17	1.03	1.14	0.77	1.20	1.16	1.11	0.95	1.00	1.01
O=F	–0.03	–0.02	–0.31	–0.18	–0.19	–0.13	–0.01	–0.16	–0.05	–0.36	–0.01	–0.08	–0.07	–0.21	–0.16	–0.16
Total	99.13	99.26	99.24	99.33	99.27	99.56	99.03	99.31	99.15	98.89	99.06	100.27	99.10	99.08	98.88	99.31
Si	3.730	3.787	3.704	3.794	3.747	3.869	3.690	3.811	3.779	3.722	3.672	3.884	3.782	3.779	3.769	3.779
Al	0.866	0.701	0.476	0.458	0.517	0.379	0.758	0.345	0.521	0.418	1.032	0.272	0.462	0.509	0.371	0.453
B	0.404	0.512	0.820	0.748	0.736	0.752	0.552	0.844	0.700	0.860	0.296	0.844	0.756	0.712	0.860	0.768
ΣTet.	5.000	5.000	5.000	5.000	5.000	5.000	5.000	5.000	5.000	5.000	5.000	5.000	5.000	5.000	5.000	5.000
Al	5.597	5.537	5.699	5.666	5.510	5.468	5.443	5.487	5.479	5.816	5.612	5.453	5.594	5.154	5.758	5.300
Mg	3.214	3.450	2.420	3.158	2.693	3.501	2.850	3.320	2.849	2.061	3.575	3.791	2.601	3.042	2.264	2.876
Fe^{2+}	0.396	0.396	0.952	0.421	0.868	0.290	0.788	0.440	0.804	1.293	0.111	0.076	0.851	0.772	1.094	0.777
Fe^{3+}	0.068	0.080	0.144	0.004	0.172	0.048	0.212	0.056	0.144	–	0.032	0.008	0.160	0.348	0.056	0.328
Mn^{2+}	–	–	–	0.014	0.038	–	0.033	0.014	–	0.013	–	–	–	–	–	–
V^{3+}	–	–	–	–	–	–	–	–	–	–	–	–	–	–	–	–
Cr^{3+}	–	–	–	–	–	–	–	–	–	–	–	–	–	–	–	–
Ti	0.011	–	–	–	–	–	–	–	0.012	0.020	–	–	0.012	0.014	0.018	–
Na	0.010	–	0.025	0.010	0.010	–	–	0.012	–	0.012	–	–	–	0.027	–	0.029
Ca	–	–	–	–	–	–	–	–	–	–	0.011	–	–	–	–	–
CATSUM	14.296	14.298	14.239	14.273	14.290	14.307	14.327	14.329	14.287	14.217	14.342	14.328	14.219	14.358	14.191	14.311
F	0.028	0.016	0.296	0.167	0.184	0.116	0.008	0.148	0.044	0.344	0.012	0.068	0.068	0.197	0.157	0.148
OH	0.972	0.984	0.704	0.833	0.816	0.884	0.992	0.852	0.956	0.656	0.988	0.932	0.932	0.803	0.843	0.852

Average of 10 points; * B *via* SREF at *T*(3); ** Fe^{3+} *via* SREF at *M*(4); *** calculated based on O_{21} $(OH+F)_1$; – : near detection limits and less than 0.01 *apfu*.

TABLE 4 (cont'd). KORNERUPINE: CHEMICAL COMPOSITIONS (wt %) AND UNIT FORMULAE (*apfu*)

	K18	K19	K20	K21	K22	K23	K24	K25	K26	K27	K28	K29	K30	K31	K32	K33
SiO_2	30.46	30.79	30.31	29.27	30.84	31.63	30.85	30.07	29.31	30.56	31.06	29.63	30.18	29.77	30.69	29.08
Al_2O_3	39.86	41.42	41.69	43.49	44.76	42.63	41.65	38.79	41.29	40.09	40.63	42.56	47.22	46.85	40.66	42.61
B_2O_3*	3.55	3.95	4.02	1.70	1.99	3.49	3.77	3.90	2.34	3.54	3.58	2.96	0.53	1.51	3.80	3.00
MgO	16.56	15.43	13.05	14.89	19.35	19.91	15.19	14.91	15.09	16.87	18.59	14.44	19.73	19.12	19.45	14.59
FeO	5.51	5.59	8.35	6.48	1.21	–	5.75	7.96	7.25	5.57	3.54	7.80	0.23	0.66	2.48	6.85
Fe_2O_3**	1.92	0.21	0.09	1.68	0.09	–	–	2.19	–	1.58	0.73	0.89	–	0.04	0.17	1.44
MnO	0.24	–	0.10	–	–	0.15	–	–	0.34	0.21	–	0.31	–	–	–	–
V_2O_3	–	0.10	0.10	–	–	0.20	0.12	–	–	–	–	–	–	–	–	–
Cr_2O_3	–	0.13	0.11	–	–	–	0.13	–	–	–	–	–	–	–	–	–
TiO_2	–	0.19	0.21	0.17	–	0.16	0.20	0.19	0.21	–	–	–	–	–	–	0.24
Na_2O	–	0.09	0.07	–	–	–	0.11	0.06	0.07	–	–	0.07	–	–	–	0.13
CaO	–	–	–	–	–	–	–	–	–	–	–	–	0.09	–	–	–
F	0.08	0.77	0.76	0.07	0.00	0.10	0.78	0.75	0.46	0.10	0.23	0.38	0.10	0.08	0.15	0.94
H_2O***	1.16	0.85	0.84	1.15	1.23	1.19	0.84	0.83	0.96	1.16	1.11	1.02	1.17	1.18	1.14	0.75
O=F	–0.03	–0.32	–0.32	–0.03	–0.00	–0.04	–0.33	–0.32	–0.19	–0.04	–0.10	–0.16	–0.04	–0.03	–0.06	–0.40
Total	99.30	99.19	99.38	98.87	99.46	99.42	99.06	99.34	99.48	99.64	99.37	99.89	99.21	99.19	98.48	99.23
Si	3.802	3.813	3.789	3.711	3.769	3.822	3.828	3.792	3.717	3.799	3.822	3.714	3.710	3.649	3.784	3.660
Al	0.434	0.343	0.343	0.917	0.811	0.450	0.364	0.360	0.771	0.441	0.418	0.646	1.178	1.031	0.408	0.688
B	0.764	0.844	0.868	0.372	0.420	0.728	0.808	0.848	0.512	0.760	0.760	0.640	0.112	0.320	0.808	0.652
ΣTet.	5.000	5.000	5.000	5.000	5.000	5.000	5.000	5.000	5.000	5.000	5.000	5.000	5.000	5.000	5.000	5.000
Al	5.430	5.703	5.799	5.581	5.636	5.620	5.727	5.405	5.400	5.433	5.475	5.641	5.663	5.738	5.501	5.632
Mg	3.082	2.849	2.432	2.814	3.525	3.586	2.810	2.803	2.853	3.127	3.410	2.698	3.616	3.494	3.576	2.737
Fe^{2+}	0.575	0.579	0.873	0.687	0.124	–	0.597	0.839	0.769	0.579	0.364	0.818	0.024	0.068	0.256	0.721
Fe^{3+}	0.180	0.020	0.008	0.160	0.008	–	–	0.208	0.224	0.148	0.068	0.084	–	0.004	0.016	0.136
Mn^{2+}	0.025	–	0.011	–	–	0.015	–	–	0.037	0.022	–	0.033	–	–	–	–
V^{3+}	–	0.010	0.010	–	–	0.019	0.012	–	–	–	–	–	–	–	–	–
Cr^{3+}	–	0.013	0.011	–	–	–	0.013	–	–	–	–	–	–	–	–	–
Ti	–	0.018	0.020	0.016	–	0.015	0.019	0.018	0.020	–	–	–	–	–	–	0.023
Na	–	0.022	0.017	–	–	–	0.026	0.015	0.017	–	–	0.017	–	–	–	0.032
Ca	–	–	–	–	–	–	–	–	–	–	–	–	0.012	–	–	–
CATSUM	14.293	14.213	14.180	14.258	14.293	14.255	14.204	14.287	14.319	14.310	14.317	14.290	14.314	14.304	14.349	14.280
F	0.032	0.302	0.300	0.028	0.000	0.038	0.306	0.299	0.184	0.039	0.090	0.151	0.039	0.031	0.058	0.374
OH	0.968	0.698	0.700	0.972	1.000	0.962	0.694	0.701	0.816	0.961	0.910	0.849	0.961	0.969	0.942	0.626

Average of 10 points; * B *via* SREF at *T*(3); ** Fe^{3+} *via* SREF at *M*(4); *** calculated based on O_{21} $(OH+F)_1$; – : near detection limits and less than 0.01 *apfu*.

of refinements. The parameters $^{T(3)}$Si and $^{T(3)}$B were refined (together with all other variables) to allow readjustment in the presence of Al at the *T* sites.

(9) The new values for B and $^{M(4)}Fe^{3+}$ were used to recalculate the unit formulae from the electron-microprobe data, producing new Si values. The Si and Al values were then updated in the refinements, and the entire refinement sequence (the tetrahedron cycle noted in Fig. 4) was iterated to self-consistency.

The secondary refinement has thus produced reasonably well-characterized site-populations for the tetrahedra, including estimates of the B and $^{[4]}$Al contents, and an approximate value for Fe^{3+}.

Tertiary refinement

The Al content of the *M* sites is given by $^{[6]}$Al = Al^{EMP} – $^{[4]}$Al. Most previous authors (Moore & Bennett 1968, Moore & Araki 1979, Finger & Hazen 1981, Klaska & Grew 1991) have reported complete occupancy of *M*(3) and *M*(5) by Al, and the mean bond-lengths of the present work are in reasonable accord with this result. Similarly, no Al has been assigned to the *M*(1), *M*(2) or *X* sites. This being the case, the Al content of *M*(4) is given by $^{[6]}$Al – 4 *apfu*. Thus at this stage of the refinement procedure, the Al occupancies of the *T*(1), *T*(2), *T*(3), *M*(3), *M*(4) and *M*(5) sites were

TABLE 4 (cont'd). KORNERUPINE: CHEMICAL COMPOSITIONS (wt %) AND UNIT FORMULAE (*apfu*)

	K34	K35	K36	K38	K39	K40	K41	K42	K43	K45	K46	K47	K49	K50	K52
SiO_2	31.07	28.66	28.53	29.68	30.60	28.95	31.67	29.63	31.05	30.91	30.71	30.51	30.18	30.20	30.78
Al_2O_3	41.62	48.04	46.90	44.91	43.76	49.57	39.27	40.98	43.73	41.33	45.88	45.14	41.20	45.59	42.79
B_2O_3*	3.59	0.09	0.20	1.48	2.29	0.08	4.21	3.70	3.15	3.66	1.55	1.71	3.28	1.60	2.85
MgO	16.22	17.72	17.96	19.21	19.55	19.42	21.74	15.34	19.58	18.41	20.38	20.24	19.41	19.26	21.24
FeO	4.94	2.71	3.09	1.76	1.82	0.49	1.16	6.86	0.07	3.26	–	–	2.99	1.06	–
Fe_2O_3**	–	0.60	1.53	0.64	0.39	0.13	0.48	0.13	0.04	0.26	–	–	0.73	0.22	0.13
MnO	–	–	–	–	–	–	–	–	0.15	0.13	–	–	–	–	–
V_2O_3	0.16	–	–	–	–	–	–	0.12	–	–	–	–	–	–	–
Cr_2O_3	0.20	–	–	0.28	0.15	–	–	–	–	–	0.26	0.25	–	–	–
TiO_2	0.21	0.12	0.13	–	–	0.13	–	0.30	0.17	–	0.15	0.12	–	–	–
Na_2O	0.14	–	–	–	–	–	–	0.07	–	0.08	–	–	–	–	–
CaO	–	0.08	–	–	–	0.09	0.09	–	–	–	0.08	0.08	–	–	–
F	0.90	0.02	0.13	0.06	0.06	0.02	0.12	0.53	0.16	0.32	0.14	0.08	0.27	0.03	0.07
H_2O***	0.79	1.19	1.14	1.18	1.20	1.21	1.18	0.94	1.16	1.07	1.17	1.19	1.08	1.21	1.20
O=F	–0.38	–0.01	–0.05	–0.03	–0.03	–0.01	–0.05	–0.22	–0.07	–0.13	–0.06	–0.03	–0.11	–0.01	–0.03
Total	99.46	99.22	99.55	99.18	99.80	100.08	99.88	98.37	99.20	99.29	100.26	99.28	99.03	99.15	99.03
Si	3.835	3.580	3.571	3.673	3.743	3.546	3.832	3.732	3.766	3.797	3.719	3.728	3.730	3.710	3.751
Al	0.401	1.400	1.385	1.011	0.773	1.438	0.288	0.464	0.574	0.427	0.957	0.912	0.570	0.950	0.649
B	0.764	0.020	0.044	0.316	0.484	0.016	0.880	0.804	0.660	0.776	0.324	0.360	0.700	0.340	0.600
ΣTet.	5.000	5.000	5.000	5.000	5.000	5.000	5.000	5.000	5.000	5.000	5.000	5.000	5.000	5.000	5.000
Al	5.653	5.673	5.533	5.538	5.535	5.718	5.312	5.619	5.678	5.557	5.591	5.588	5.432	5.652	5.498
Mg	2.984	3.300	3.351	3.544	3.565	3.546	3.921	2.880	3.541	3.372	3.679	3.686	3.576	3.528	3.859
Fe^{2+}	0.510	0.283	0.323	0.182	0.186	0.050	0.117	0.723	0.007	0.335	–	–	0.309	0.109	–
Fe^{3+}	–	0.056	0.144	0.060	0.036	0.012	0.044	0.012	0.004	0.024	–	–	0.068	0.020	0.012
Mn^{2+}	–	–	–	–	–	–	–	–	0.015	0.014	–	–	–	–	–
V^{3+}	0.016	–	–	–	–	–	–	0.012	–	–	–	–	–	–	–
Cr^{3+}	0.020	–	–	0.027	0.015	–	–	–	–	–	0.025	0.024	–	–	–
Ti	0.019	0.011	0.012	–	–	0.012	–	0.028	0.016	–	0.014	0.011	–	–	–
Na	0.034	–	–	–	–	–	–	0.017	–	0.019	–	–	–	–	–
Ca	–	0.011	–	–	–	0.012	0.012	–	–	–	0.010	0.010	–	–	–
CATSUM	14.236	14.334	14.364	14.351	14.336	14.350	14.406	14.292	14.260	14.320	14.319	14.319	14.385	14.309	14.369
F	0.351	0.008	0.051	0.023	0.023	0.008	0.046	0.211	0.061	0.124	0.054	0.031	0.106	0.012	0.027
OH	0.649	0.992	0.949	0.977	0.977	0.992	0.954	0.789	0.939	0.876	0.946	0.969	0.894	0.988	0.973

Average of 10points; * B *via* SREF at *T*(3); ** Fe^{3+} *via* SREF at *M*(4); *** calculated based on $O_{21}(OH+F)_1$; –: near detection limits and less than 0.01 *apfu*.

TABLE 5. SREF SCATTERING-FACTOR ASSIGNMENT IN KORNERUPINE

Site	□	B	O^{2-}	F^-	Na	Mg	Al	Si	Ca	Ti	V	Cr	Fe
X	*				F	AR			F				AR
M(1)						R							R
M(2)						R	EX						R
M(3)						EX	F						
M(4)						R	F			F	F	F	R
M(5)						EX	F						
T(1)							F	F					
T(2)							F	F					
T(3)		R					F	R					
O(10)			R	R									

*: only *X*-site vacancies are considered; R: refined occupancy-factor; F: fixed occupancy-factor; AR: alternative refined occupancy-factors [this indicates that the scattering from (Mg + Fe) was refined first as variable Mg and in a second phase of refinement as variable Fe, see text]; EX: minor occupant of site excluded in refinements.

fixed. On the basis of the observed mean bond-lengths and refined site-scattering parameters, the (minor) Ti, V and Cr contents of the unit formulae were assigned to the *M*(4) site. Subsequent steps were as follows:

(1) The Mg and Fe contents of the *M*(4) site were then determined by refinement; this step also leads to new Fe^{3+} and possibly new B values.

(2) The new Fe^{3+} and B values are used to recalculate the formula from the electron-microprobe data.

(3) If the Si value changes, then the tetrahedron cycle of refinement (Secondary Refinement, Fig. 4) is repeated to self-consistency.

(4) The tertiary refinement is then repeated with updated values of $^{M(4)}$Al.

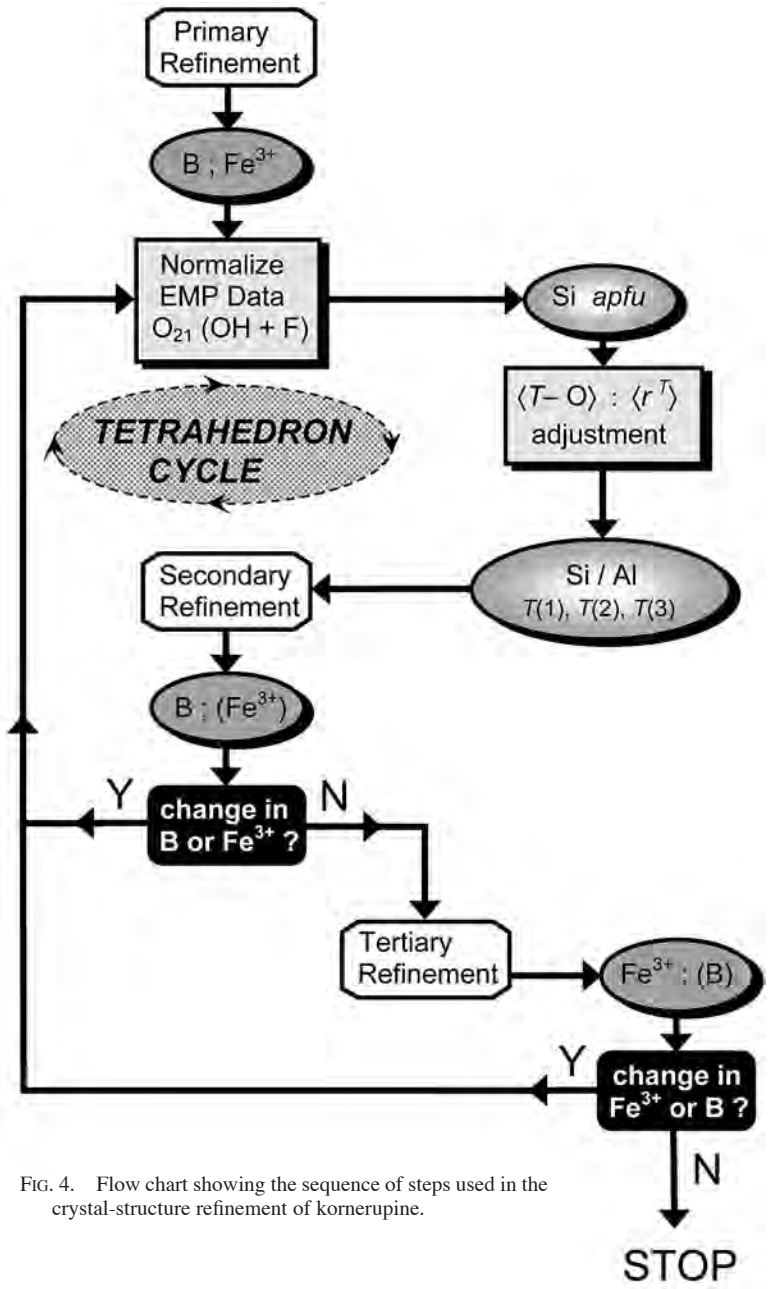

FIG. 4. Flow chart showing the sequence of steps used in the crystal-structure refinement of kornerupine.

(5) The secondary and tertiary stages of the refinement process are run to self-consistency.

(6) The Mg and Fe^{2+} contents of the *X* site are assigned as ${}^{X}Mg = {}^{EMP}Mg - {}^{M}Mg$ and ${}^{X}Fe^{2+} = {}^{EMP}Fe^{2+} - {}^{M}Fe^{2+}$.

This completes the refinement process, and at this stage, the results of the site-scattering refinement and the electron-microprobe compositions are completely conformable within experimental uncertainty. Minor readjustments of site populations remain to be made *via* the development of relations between mean bond-length and constituent-cation radius.

Determination of B by SIMS

Hawthorne *et al.* (1995) determined the B content in kornerupine using a subset of the samples used here (K1–K32) and compared the results with the B content determined by SREF. As the physical bases of SIMS and SREF are independent, there should be no systematic error common to each method, allowing accurate assignment of both precision and accuracy. The agreement between the results of the two methods is as follows (Fig. 5): SREF, 1–2% relative, 0.01–0.08 wt% absolute; SIMS, 1–2% relative, 0.01–0.08 wt% absolute, with an overall agreement within 3% relative. Thus the methods are accurate to within the limits of their assigned precision (*i.e.*, 3% relative). The B contents of the remaining crystals of kornerupine (K33–K52) were determined by SREF, and a similar accuracy and precision for B content are expected for these crystals.

TABLE 6. KORNERUPINE: SELECTED INTERATOMIC DISTANCES (Å)

		K1	K2	K3	K5	K6	K7	K8	K9	K10	K11	K12	K13	K14	K15	K16	K17
X–O(4),a,b,c	×4	2.641	2.635	2.633	2.623	2.625	2.618	2.634	2.617	2.633	2.628	2.635	2.609	2.635	2.633	2.635	2.635
X–O(9)d,e	×2	2.311	2.304	2.330	2.315	2.314	2.297	2.310	2.304	2.311	2.340	2.308	2.293	2.321	2.294	2.330	2.301
X–O(10),b	×2	2.069	2.068	2.080	2.068	2.075	2.076	2.072	2.076	2.068	2.070	2.067	2.065	2.060	2.095	2.059	2.086
<*X*–O>		2.416	2.411	2.419	2.407	2.410	2.402	2.413	2.404	2.411	2.417	2.411	2.394	2.413	2.414	2.415	2.414
M(1)–O(1)		2.118	2.123	2.159	2.143	2.141	2.132	2.127	2.141	2.139	2.165	2.104	2.134	2.151	2.137	2.160	2.142
M(1)–O(4),f	×2	2.119	2.116	2.117	2.114	2.122	2.113	2.125	2.115	2.120	2.119	2.119	2.111	2.123	2.120	2.120	2.119
M(1)–O(5)		2.259	2.231	2.230	2.220	2.217	2.199	2.224	2.190	2.227	2.235	2.249	2.175	2.232	2.214	2.237	2.216
M(1)–O(7)		2.057	2.069	2.115	2.099	2.108	2.098	2.088	2.105	2.107	2.127	2.033	2.099	2.114	2.107	2.127	2.113
M(1)–O(10)		2.044	2.050	1.980	2.009	2.017	2.027	2.044	2.017	2.021	1.975	2.078	2.041	2.004	2.021	1.980	2.011
<*M*(1)–O>		2.119	2.118	2.120	2.117	2.121	2.114	2.122	2.114	2.122	2.123	2.117	2.112	2.125	2.120	2.124	2.120
M(2)–O(2),g	×2	2.078	2.074	2.091	2.076	2.081	2.067	2.076	2.068	2.078	2.103	2.077	2.062	2.081	2.073	2.089	2.075
M(2)–O(3),g	×2	1.993	1.992	2.002	1.995	1.997	1.992	1.993	1.994	1.994	2.008	1.991	1.994	1.999	1.992	1.999	1.996
M(2)–O(8),f	×2	2.192	2.201	2.247	2.230	2.237	2.224	2.221	2.243	2.231	2.256	2.178	2.232	2.239	2.231	2.253	2.237
<*M*(2)–O>		2.088	2.089	2.113	2.101	2.105	2.094	2.097	2.102	2.101	2.122	2.082	2.096	2.106	2.099	2.114	2.103
M(3)–O(1),h	×2	1.797	1.795	1.793	1.793	1.796	1.792	1.797	1.792	1.795	1.794	1.797	1.791	1.796	1.794	1.796	1.794
M(3)–O(4),a	×2	1.872	1.871	1.857	1.863	1.866	1.867	1.876	1.864	1.867	1.855	1.882	1.870	1.859	1.868	1.850	1.865
M(3)–O(6),a	×2	2.111	2.113	2.117	2.113	2.109	2.110	2.105	2.107	2.111	2.116	2.106	2.106	2.115	2.116	2.116	2.115
<*M*(3)–O>		1.927	1.926	1.922	1.923	1.924	1.923	1.926	1.922	1.924	1.922	1.928	1.922	1.923	1.926	1.921	1.925
M(4)–O(1)		1.934	1.935	1.909	1.916	1.928	1.931	1.939	1.924	1.928	1.893	1.942	1.929	1.918	1.949	1.897	1.941
M(4)–O(2)		1.933	1.937	1.925	1.928	1.936	1.937	1.945	1.932	1.937	1.917	1.931	1.938	1.934	1.959	1.918	1.950
M(4)–O(3)		1.895	1.897	1.865	1.878	1.885	1.891	1.901	1.885	1.886	1.857	1.904	1.890	1.877	1.908	1.857	1.896
M(4)–O(5)		1.808	1.823	1.825	1.832	1.833	1.844	1.824	1.846	1.833	1.825	1.801	1.852	1.830	1.850	1.827	1.846
M(4)–O(6),f	×2	2.085	2.088	2.082	2.087	2.093	2.095	2.093	2.095	2.094	2.083	2.081	2.095	2.091	2.105	2.085	2.099
<*M*(4)–O>		1.957	1.961	1.948	1.955	1.961	1.966	1.966	1.963	1.962	1.943	1.957	1.967	1.957	1.979	1.945	1.972
M(5)–O(2),h	×2	1.799	1.797	1.801	1.798	1.803	1.798	1.801	1.800	1.801	1.802	1.798	1.798	1.802	1.800	1.803	1.801
M(5)–O(6),a	×2	1.991	1.994	2.004	2.003	1.999	2.002	1.988	2.004	1.998	2.009	1.985	2.005	2.000	1.998	2.003	2.000
M(5)–O(8),i	×2	1.949	1.946	1.933	1.935	1.937	1.936	1.949	1.932	1.938	1.930	1.957	1.934	1.935	1.939	1.928	1.938
<*M*(5)–O>		1.913	1.912	1.913	1.912	1.913	1.912	1.913	1.912	1.912	1.914	1.913	1.912	1.912	1.912	1.911	1.913
T(1)–O(3)		1.621	1.623	1.624	1.620	1.620	1.617	1.619	1.615	1.622	1.624	1.624	1.616	1.619	1.617	1.622	1.620
T(1)–O(4)e,j	×2	1.619	1.619	1.613	1.613	1.616	1.613	1.617	1.614	1.616	1.612	1.620	1.614	1.616	1.617	1.613	1.616
T(1)–O(9)		1.639	1.637	1.624	1.629	1.633	1.632	1.640	1.630	1.634	1.622	1.643	1.634	1.630	1.635	1.624	1.632
<*T*(1)–O>		1.625	1.625	1.619	1.619	1.621	1.619	1.623	1.618	1.622	1.618	1.627	1.620	1.620	1.622	1.618	1.621
T(2)–O(5)		1.609	1.608	1.609	1.603	1.609	1.599	1.617	1.600	1.608	1.605	1.615	1.599	1.607	1.604	1.603	1.605
T(2)–O(6)e,j	×2	1.685	1.677	1.672	1.667	1.674	1.662	1.682	1.664	1.672	1.668	1.695	1.659	1.672	1.668	1.669	1.668
T(2)–O(7)		1.695	1.689	1.676	1.676	1.681	1.671	1.695	1.672	1.678	1.673	1.705	1.671	1.676	1.677	1.670	1.677
<*T*(2)–O>		1.669	1.663	1.657	1.653	1.660	1.649	1.670	1.650	1.657	1.654	1.678	1.648	1.657	1.654	1.653	1.655
T(3)–O(7),k	×2	1.560	1.537	1.484	1.492	1.491	1.494	1.522	1.481	1.499	1.479	1.589	1.483	1.490	1.497	1.478	1.488
T(3)–O(8)e,j	×2	1.627	1.608	1.552	1.564	1.573	1.563	1.599	1.542	1.576	1.542	1.643	1.543	1.567	1.572	1.543	1.564
<*T*(3)–O>		1.594	1.573	1.518	1.528	1.533	1.529	1.561	1.512	1.538	1.511	1.616	1.513	1.528	1.535	1.511	1.526

Symmetry operators: a: $x,-y,-z$; b: $-x,-y,-z$; c: $-x,y,z$; d: $x-\frac{1}{2},y-\frac{1}{2},z$; e: $-x+\frac{1}{2},-y+\frac{1}{2},-z$; f: $x,y,-z+\frac{1}{2}$; g: $-x+1,y,-z+\frac{1}{2}$; h: $x,-y,z-\frac{1}{2}$; i: $-x+1,-y,-z$; j: $-x+\frac{1}{2},-y+\frac{1}{2},z+\frac{1}{2}$; k: $-x,y,-z+\frac{1}{2}$. The e.s.d. are ≤0.002 Å for individual distances.

TABLE 6 (cont'd). KORNERUPINE: SELECTED INTERATOMIC DISTANCES (Å)

		K18	K19	K20	K21	K22	K23	K24	K25	K26	K27	K28	K29	K30	K31	K32	K33
X–O(4),a,b,c	×4	2.631	2.627	2.631	2.648	2.637	2.624	2.630	2.624	2.633	2.627	2.620	2.627	2.642	2.635	2.617	2.634
X–O(9)d,e	×2	2.301	2.322	2.335	2.314	2.309	2.308	2.326	2.308	2.311	2.302	2.301	2.321	2.313	2.314	2.300	2.325
X–O(10),b	×2	2.070	2.082	2.065	2.069	2.064	2.061	2.087	2.093	2.089	2.070	2.074	2.070	2.068	2.062	2.066	2.102
<*X*–O>		2.408	2.415	2.416	2.420	2.412	2.404	2.418	2.412	2.417	2.407	2.404	2.411	2.416	2.412	2.400	2.424
M(1)–O(1)		2.140	2.155	2.163	2.120	2.118	2.139	2.155	2.147	2.124	2.137	2.136	2.139	2.095	2.109	2.137	2.143
M(1)–O(4),f	×2	2.118	2.112	2.118	2.124	2.115	2.113	2.112	2.117	2.123	2.118	2.117	2.120	2.117	2.116	2.114	2.117
M(1)–O(5)		2.212	2.221	2.233	2.286	2.260	2.208	2.237	2.204	2.237	2.205	2.197	2.227	2.292	2.257	2.194	2.234
M(1)–O(7)		2.106	2.109	2.120	2.059	2.049	2.086	2.108	2.118	2.075	2.105	2.099	2.094	2.007	2.027	2.101	2.087
M(1)–O(10)		2.024	1.980	1.976	2.035	2.050	2.027	1.973	2.000	2.034	2.027	2.030	2.019	2.081	2.061	2.031	1.998
<*M*(1)–O>		2.120	2.115	2.121	2.124	2.118	2.114	2.116	2.117	2.119	2.118	2.116	2.120	2.118	2.114	2.115	2.116
M(2)–O(2),g	×2	2.072	2.082	2.091	2.085	2.076	2.069	2.087	2.080	2.082	2.071	2.067	2.084	2.082	2.077	2.066	2.091
M(2)–O(3),g	×2	1.994	1.997	2.003	1.994	1.992	1.993	1.997	1.996	1.994	1.994	1.994	1.998	1.994	1.990	1.995	1.999
M(2)–O(8),f	×2	2.234	2.244	2.251	2.193	2.186	2.221	2.239	2.248	2.211	2.234	2.231	2.230	2.153	2.177	2.230	2.230
<*M*(2)–O>		2.100	2.108	2.115	2.091	2.085	2.094	2.108	2.108	2.096	2.100	2.098	2.104	2.076	2.081	2.097	2.107
M(3)–O(1),h	×2	1.794	1.793	1.795	1.799	1.797	1.793	1.795	1.793	1.796	1.794	1.793	1.795	1.798	1.796	1.792	1.795
M(3)–O(4),a	×2	1.865	1.854	1.853	1.871	1.869	1.862	1.855	1.862	1.873	1.867	1.869	1.867	1.881	1.874	1.867	1.866
M(3)–O(6),a	×2	2.112	2.119	2.119	2.113	2.115	2.115	2.121	2.112	2.108	2.110	2.108	2.106	2.109	2.106	2.109	2.113
<*M*(3)–O>		1.924	1.922	1.922	1.928	1.927	1.923	1.924	1.922	1.926	1.923	1.923	1.923	1.929	1.926	1.923	1.925
M(4)–O(1)		1.931	1.907	1.894	1.937	1.928	1.919	1.903	1.930	1.945	1.931	1.930	1.919	1.942	1.929	1.924	1.923
M(4)–O(2)		1.942	1.923	1.919	1.934	1.927	1.928	1.920	1.942	1.940	1.940	1.938	1.928	1.921	1.919	1.934	1.929
M(4)–O(3)		1.889	1.865	1.857	1.893	1.891	1.881	1.864	1.886	1.902	1.891	1.891	1.881	1.902	1.891	1.887	1.878
M(4)–O(5)		1.841	1.831	1.825	1.799	1.810	1.834	1.829	1.845	1.817	1.844	1.844	1.821	1.787	1.793	1.848	1.819
M(4)–O(6),f	×2	2.097	2.085	2.083	2.086	2.083	2.086	2.085	2.099	2.092	2.097	2.095	2.084	2.075	2.073	2.093	2.084
<*M*(4)–O>		1.966	1.949	1.944	1.956	1.954	1.956	1.948	1.967	1.964	1.967	1.966	1.953	1.950	1.946	1.963	1.953
M(5)–O(2),h	×2	1.800	1.800	1.802	1.800	1.797	1.797	1.800	1.802	1.801	1.801	1.799	1.801	1.797	1.797	1.799	1.801
M(5)–O(6),a	×2	2.000	2.006	2.007	1.989	1.993	2.002	2.008	2.005	1.991	2.000	2.000	1.995	1.985	1.983	2.004	1.998
M(5)–O(8),i	×2	1.938	1.931	1.931	1.951	1.946	1.936	1.931	1.933	1.945	1.938	1.936	1.940	1.962	1.951	1.935	1.940
<*M*(5)–O>		1.913	1.912	1.913	1.913	1.912	1.912	1.913	1.913	1.912	1.913	1.912	1.912	1.915	1.910	1.913	1.913
T(1)–O(3)		1.619	1.622	1.624	1.624	1.623	1.620	1.624	1.621	1.621	1.618	1.616	1.621	1.624	1.624	1.615	1.624
T(1)–O(4)e,j	×2	1.616	1.615	1.612	1.619	1.620	1.615	1.615	1.616	1.618	1.615	1.614	1.616	1.622	1.620	1.614	1.617
T(1)–O(9)		1.635	1.622	1.622	1.640	1.638	1.630	1.621	1.628	1.635	1.635	1.634	1.633	1.643	1.637	1.635	1.628
<*T*(1)–O>		1.622	1.619	1.618	1.626	1.625	1.620	1.619	1.620	1.623	1.621	1.620	1.622	1.628	1.625	1.620	1.622
T(2)–O(5)		1.606	1.600	1.606	1.615	1.605	1.601	1.598	1.604	1.616	1.603	1.603	1.611	1.610	1.613	1.599	1.610
T(2)–O(6)e,j	×2	1.666	1.666	1.668	1.689	1.681	1.667	1.665	1.666	1.683	1.668	1.666	1.680	1.698	1.695	1.662	1.681
T(2)–O(7)		1.678	1.673	1.671	1.698	1.691	1.675	1.671	1.670	1.693	1.675	1.674	1.687	1.710	1.699	1.672	1.686
<*T*(2)–O>		1.655	1.651	1.653	1.673	1.665	1.653	1.650	1.652	1.669	1.654	1.652	1.665	1.680	1.676	1.649	1.665
T(3)–O(7),k	×2	1.489	1.481	1.480	1.573	1.562	1.497	1.486	1.480	1.536	1.492	1.491	1.507	1.633	1.585	1.487	1.511
T(3)–O(8)e,j	×2	1.563	1.546	1.543	1.634	1.629	1.571	1.558	1.547	1.613	1.564	1.561	1.584	1.671	1.643	1.551	1.587
<*T*(3)–O>		1.526	1.514	1.512	1.604	1.596	1.534	1.522	1.514	1.575	1.528	1.526	1.546	1.652	1.614	1.519	1.549

Symmetry operators: a: $x,-y,-z$; b: $-x,-y,-z$; c: $-x,y,z$; d: $x-\frac{1}{2},y-\frac{1}{2},z$; e: $-x+\frac{1}{2},-y+\frac{1}{2},-z$; f: $x,y,-z+\frac{1}{2}$; g: $-x+1,y,-z+\frac{1}{2}$; h: $x,-y,z-\frac{1}{2}$; i: $-x+1,-y,-z$; j: $-x+\frac{1}{2},-y+\frac{1}{2},z+\frac{1}{2}$; k: $-x,y,-z+\frac{1}{2}$. The e.s.d. are ≤0.002 Å for individual distances.

Determination of Fe^{3+} by Mössbauer Spectroscopy

Grew *et al.* (1999) examined a subset of six samples of the kornerupine crystals used here by ^{57}Fe Mössbauer spectroscopy. It was not possible to determine the Fe^{3+} contents in kornerupine directly because of the close overlap of the individual bands in the spectra. However, incorporation of the Fe^{3+} contents determined by SREF and crystal-chemical analysis as done here allowed accurate fitting of the spectra, showing that the Fe^{3+} contents determined by SREF are in accord with the Mössbauer spectra of the same samples.

TABLE 6 (cont'd). KORNERUPINE: SELECTED INTERATOMIC DISTANCES (Å)

		K34	K35	K36	K38	K39	K40	K41	K42	K43	K45	K46	K47	K49	K50	K52
X–O(4),a,b,c	×4	2.633	2.651	2.644	2.638	2.634	2.646	2.604	2.623	2.629	2.619	2.634	2.631	2.616	2.639	2.620
X–O(9)d,e	×2	2.321	2.327	2.318	2.310	2.306	2.322	2.284	2.318	2.312	2.305	2.308	2.307	2.297	2.306	2.293
X–O(10),b	×2	2.097	2.073	2.081	2.070	2.068	2.067	2.069	2.075	2.061	2.074	2.069	2.066	2.075	2.065	2.065
<*X*–O>		2.421	2.426	2.422	2.414	2.411	2.420	2.390	2.410	2.408	2.404	2.411	2.409	2.401	2.412	2.400
M(1)–O(1)		2.153	2.094	2.091	2.107	2.119	2.091	2.126	2.146	2.136	2.137	2.112	2.112	2.125	2.111	2.117
M(1)–O(4),f	×2	2.113	2.124	2.125	2.122	2.118	2.124	2.115	2.118	2.115	2.112	2.115	2.117	2.115	2.114	2.114
M(1)–O(5)		2.242	2.299	2.272	2.244	2.229	2.281	2.158	2.209	2.219	2.206	2.262	2.255	2.192	2.268	2.205
M(1)–O(7)		2.105	2.010	2.011	2.038	2.065	2.000	2.104	2.107	2.076	2.100	2.036	2.039	2.089	2.037	2.072
M(1)–O(10)		1.979	2.084	2.094	2.079	2.062	2.097	2.052	2.005	2.030	2.016	2.060	2.061	2.042	2.056	2.059
<*M*(1)–O>		2.118	2.123	2.120	2.119	2.118	2.120	2.111	2.117	2.115	2.114	2.117	2.117	2.113	2.117	2.114
M(2)–O(2),g	×2	2.088	2.087	2.083	2.077	2.074	2.084	2.054	2.079	2.070	2.069	2.079	2.077	2.067	2.079	2.067
M(2)–O(3),g	×2	1.999	1.997	1.998	1.995	1.995	1.997	1.994	1.997	1.996	1.995	1.991	1.993	1.994	1.992	1.994
M(2)–O(8),f	×2	2.233	2.154	2.161	2.185	2.200	2.155	2.238	2.241	2.216	2.231	2.178	2.182	2.224	2.179	2.206
<*M*(2)–O>		2.107	2.079	2.081	2.086	2.090	2.079	2.095	2.106	2.094	2.098	2.083	2.084	2.095	2.083	2.089
M(3)–O(1),h	×2	1.795	1.803	1.801	1.799	1.796	1.801	1.792	1.794	1.794	1.793	1.797	1.797	1.793	1.797	1.794
M(3)–O(4),a	×2	1.859	1.888	1.892	1.883	1.876	1.889	1.871	1.862	1.865	1.863	1.876	1.877	1.872	1.874	1.873
M(3)–O(6),a	×2	2.125	2.103	2.096	2.107	2.112	2.098	2.100	2.110	2.115	2.112	2.113	2.112	2.104	2.113	2.109
<*M*(3)–O>		1.926	1.931	1.930	1.930	1.928	1.929	1.921	1.922	1.925	1.922	1.929	1.929	1.923	1.928	1.925
M(4)–O(1)		1.914	1.945	1.957	1.945	1.939	1.943	1.937	1.914	1.921	1.920	1.939	1.936	1.935	1.933	1.938
M(4)–O(2)		1.925	1.922	1.931	1.934	1.935	1.918	1.943	1.925	1.926	1.932	1.928	1.931	1.939	1.927	1.939
M(4)–O(3)		1.873	1.905	1.914	1.908	1.901	1.907	1.897	1.874	1.881	1.880	1.899	1.899	1.893	1.894	1.901
M(4)–O(5)		1.835	1.776	1.779	1.803	1.821	1.773	1.861	1.834	1.826	1.842	1.806	1.808	1.841	1.802	1.840
M(4)–O(6),f	×2	2.088	2.074	2.076	2.085	2.088	2.069	2.102	2.089	2.085	2.090	2.084	2.085	2.094	2.081	2.093
<*M*(4)–O>		1.954	1.949	1.956	1.960	1.962	1.947	1.974	1.954	1.954	1.959	1.957	1.957	1.966	1.953	1.967
M(5)–O(2),h	×2	1.801	1.802	1.802	1.801	1.800	1.801	1.800	1.801	1.798	1.798	1.797	1.797	1.798	1.796	1.797
M(5)–O(6),a	×2	2.010	1.981	1.974	1.985	1.993	1.976	2.005	2.004	2.000	2.003	1.993	1.993	1.998	1.991	1.998
M(5)–O(8),i	×2	1.935	1.972	1.974	1.958	1.951	1.972	1.933	1.933	1.940	1.934	1.951	1.951	1.938	1.950	1.942
<*M*(5)–O>		1.915	1.918	1.917	1.914	1.915	1.916	1.913	1.913	1.913	1.912	1.914	1.914	1.911	1.912	1.912
T(1)–O(3)		1.624	1.629	1.626	1.623	1.620	1.626	1.612	1.620	1.620	1.617	1.624	1.622	1.616	1.623	1.615
T(1)–O(4)e,j	×2	1.616	1.626	1.625	1.622	1.620	1.624	1.615	1.613	1.616	1.615	1.620	1.619	1.615	1.619	1.618
T(1)–O(9)		1.625	1.646	1.648	1.645	1.641	1.647	1.636	1.627	1.632	1.631	1.639	1.639	1.635	1.640	1.639
<*T*(1)–O>		1.620	1.632	1.631	1.628	1.625	1.630	1.620	1.618	1.621	1.620	1.626	1.625	1.620	1.625	1.623
T(2)–O(5)		1.598	1.623	1.629	1.620	1.609	1.625	1.599	1.606	1.604	1.597	1.608	1.608	1.603	1.608	1.599
T(2)–O(6)e,j	×2	1.666	1.714	1.717	1.695	1.682	1.717	1.657	1.666	1.670	1.664	1.685	1.683	1.668	1.685	1.670
T(2)–O(7)		1.672	1.724	1.730	1.708	1.695	1.727	1.669	1.676	1.679	1.672	1.693	1.692	1.678	1.695	1.680
<*T*(2)–O>		1.651	1.694	1.698	1.680	1.667	1.697	1.646	1.653	1.656	1.649	1.668	1.667	1.654	1.668	1.655
T(3)–O(7),k	×2	1.495	1.648	1.638	1.583	1.542	1.646	1.479	1.487	1.512	1.489	1.584	1.578	1.499	1.582	1.522
T(3)–O(8)e,j	×2	1.569	1.681	1.674	1.641	1.615	1.679	1.532	1.552	1.582	1.557	1.639	1.634	1.572	1.639	1.594
<*T*(3)–O>		1.532	1.665	1.656	1.612	1.579	1.663	1.505	1.520	1.547	1.523	1.611	1.606	1.536	1.611	1.558

Symmetry operators: a: *x*,–*y*,–*z*; b: –*x*,–*y*,–*z*; c: –*x*,*y*,*z*; d: *x*–½,*y*–½,*z*; e: –*x*+½,–*y*+½,–*z*; f: *x*,*y*,–*z*+½; g: –*x*+1,*y*,–*z*+½; h: *x*,–*y*,*z*–½; i: –*x*+1,–*y*,–*z*; j: –*x*+½,–*y*+½,*z*+½; k:–*x*,*y*,–*z*+½. The e.s.d. are ≤0.002 Å for individual distances.

Final Assignment of Site Populations: The *T* Sites

During the refinement process, the site populations at the *T*(1) and *T*(2) sites were assigned such that they fit exactly the postulated relations between <*T*–O> and <*r*> at these sites; the correctness of this process was evaluated *via* the relation between <*T*(3)–O> and $<r^{T(3)}>$. In this procedure, all relative error associated with these relations has accumulated at the *T*(3) site. As this distribution of error is inappropriate, the deviations from linearity for the *T*(3) relation were subsequently distributed among the three *T* sites in accord with their respective multiplicities. The resulting site-populations are given in Table 7, and the <*T*–O> – <*r*> relations are shown in Figure 6. Linear regression gave r^2 values in

the range 0.927–0.998, the lower r^2 values being for the *T* sites with smaller ranges of <*T*–O> values; the regression models are given in Table 8. The *y* intercepts are in the range 1.36–1.37 Å, and the slopes of the regression lines are in the range 1.00–1.02, in agreement with the *hard-sphere model* (*i.e.*, $<T\text{–O}> = <r^{\text{CATION}}> + <r^{\text{ANION}}>$; values for cation and anion radii were taken from Shannon 1976).

Final Assignment of Site Populations: The *M* Sites

The principal chemical variables at the *M* sites are Al, Mg, Fe^{2+} and Fe^{3+}. During site-scattering refinement, we made some assumptions about the site populations of these species. The mean bond-lengths reported here (and in previous work) are more or less in accord with these assumptions. However, now we are in a position to test these assumptions more rigorously, and possibly to reassign the site populations somewhat in light of the mean bond-length data available for all forty-seven crystals of kornerupine.

Preliminary considerations

The M(2) site: At the present stage, the *M*(2) site is occupied by Mg and Fe^{2+}. Figure 7 shows the variation in <*M*(2)–O> as a function of mean constituent-cation radius. The data define a field that can be outlined by an acute scalene triangle (labeled ABC in Fig. 7). At a constituent-cation radius of 0.72 Å (= Mg), the data plot over a continuous range from 2.075 to 2.095 Å. Let us postulate that the relation between <*M*(2)–O> and $<r^{M(2)}>$ conforms to a hard-sphere model. The mean radius of the anions coordinating *M*(2) is 1.373 Å. Adding this anion radius to that of Mg (0.72 Å) gives a sum of 2.093 Å, close to point A in Figure 7. The data along the AB edge of the triangle in Figure 7 define a line with a slope of ~1.0, and thus a hard sphere model of Mg ⇌ Fe^{2+} substitution at *M*(2) is conformable with the data lying just below the line AB. The remainder of the data have <*M*(2)–O> distances shorter than those predicted by their (Mg, Fe^{2+}) site-populations. This feature can be explained by incorporation of a third cation at *M*(2), a cation that has a smaller radius than Mg. The possible candidates (Table 4) are Al and Fe^{3+}. However, we may rule out Fe^{3+}, as the data near vertex C (Fig. 7) contain no appreciable Fe at *M*(2), as indicated by site-scattering refinement (Table 7; <*M*(2)–O> ≤ 2.085 Å, site-scattering < 12.57 *epfu*, mean value 12.34 *apfu*). Furthermore, we assume that Fe^{3+} is absent from *M*(2) in all crystals, as deviation from a hard-sphere model (~AB, Fig. 7) *decreases* with *increasing* Fe content at *M*(2). Thus we conclude that the deviations from a hard-sphere model of Mg ⇌ Fe^{2+} occupancy only at the *M*(2) site indicated in Figure 7 are actually due to the incorporation of Al at *M*(2) in addition to Mg and Fe^{2+}. The Al is assigned to the *M*(2) site such that a linear $<M(2)\text{–O}> - <r^{M(2)}>$ variation (with a slope of close to 1.0) is obtained.

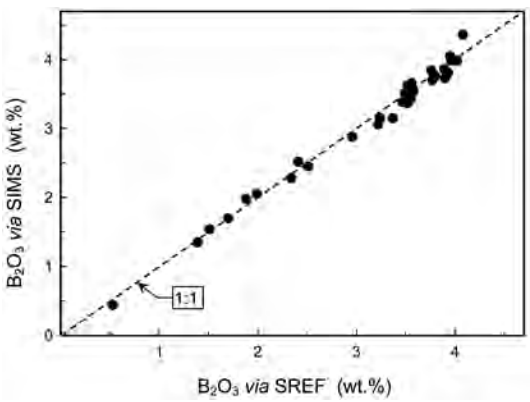

FIG. 5. Comparison of B_2O_3 (wt.%) determined by SIMS and SREF in kornerupine; the dashed reference-line has a slope of 1. Samples K1 → K32.

The M(3) and M(5) sites: At all stages of refinement, the *M*(3) and *M*(5) sites were completely occupied by Al. At the end of the secondary stage of refinement, these assumptions were tested by refining the following models: (1) *M*(3) occupancy fixed as Al, *M*(5) occupancy variable; (2) *M*(5) occupancy fixed as Al, *M*(3) occupancy variable; (3) both *M*(3) and *M*(5) occupancies variable; in addition, all other structure variables were refined simultaneously. In all cases, the refined site-scattering values at the *M*(3) and *M*(5) sites showed no significant deviations from 13 electrons per site (= 1.0 Al).

Figure 8 shows the variation in <*M*(3)–O> and <*M*(5)–O> in kornerupine. The sequence of crystals is ordered from left to right in terms of increasing <*M*(3)–O>; note that the <*M*(5)–O> values order in exactly the same way. Usually, such small and systematic variations in structures are attributed to "steric adjustments". However, let us examine the possibility of another substituent at these sites. The only reasonable substituent is Mg; any other cations of reasonable radius would not be in accord with the observed site-scattering values of 13 e per site. Thus small amounts of Mg were assigned to *M*(3) and *M*(5) to account for the variations in <*M*(3)–O> and <*M*(5)–O> throughout the complete set of data.

Comparison of M(2), M(3) and M(5) site-populations: There is an approximate 1:1 relation between the Al assigned to *M*(2) and the Mg assigned to *M*(3) and *M*(5), suggesting that the minor occupancies are responsible for the observed scatter in Figure 7 and the variations in <*M*(3)–O> and <*M*(5)–O> in Figure 8.

Final M-site assignments

Final assignment of site populations to the *M* sites involves examination of the <*M*–O> bond-lengths as a function of constituent site-occupancies.

The M(2), M(3), M(4) and M(5) sites: At this stage, $^{M(4)}$[Fe^{3+},Cr,V,Ti], $^{M(2)}Fe^{2+}$ and $^{[6]}$Al are known, and the Mg/Al values at the *M*(2), *M*(3), *M*(4) and *M*(5) sites need to be optimized for linearity on <*M*–O> *versus* <*r*> plots. This was done in the following manner:

(1) For the *M*(3) and *M*(5) sites, a slope of 1.0 is assumed initially for the <*M*–O> *versus* <*r*> relations; $^{M(3)}$Al, $^{M(3)}$Mg, $^{M(5)}$Al and $^{M(5)}$Mg values are then calculated for two intercept values, one for *M*(3) and one for *M*(5).

(2) For the *M*(4) site, $^{M(4)}$Al and $^{M(4)}$Mg were calculated for a range of values for the slope and intercept.

(3) For each set of occupancies determined in (2), a new value of $^{M(2)}$Al is produced from the relation $^{M(2)}Al = {}^{[6]}Al - {}^{M(3)}Al - {}^{M(4)}Al - {}^{M(5)}Al$. The resulting <*M*(2)–O> *versus* <$r^{M(2)}$> relation is then compared to Figure 7 for relative improvement or deterioration of agreement with a linear model.

The cycle (1) → (3) was iterated for various values of intercepts for *M*(3) and *M*(5) and for various site-occupancy possibilities: (i) Mg at *M*(3), (ii) Mg at *M*(5), (iii) Mg at *M*(3) and *M*(5), and (iv) no Mg at *M*(3) or *M*(5). Note that the adjustment of Al/Mg in the sequence *M*(3), *M*(5) → *M*(4) → *M*(2) takes advantage of the relative multiplicities of the sites involved [2:2:2:1] in that small changes in *M*(3), *M*(5) and *M*(4) result in larger changes at *M*(2). The *M*(3), *M*(5) and *M*(4) site-populations that gave the best relation for the *M*(2) site are considered to be the optimum values. Changes to $^{M(4)}$Al were tested to see if they changed the $^{M(4)}$Fe values (as $^{M(4)}Fe = Fe^{3+}$, any change would require recalculation of the unit formula and a repeat of the tertiary cycle of refinement); however, there was no change in $^{M(4)}$Fe for any of the refinements.

For these sites, the final stage involves adjustment of the site populations slightly such that for a specific crystal, each site shows the same deviation from the <*M*–O> – <*r*> relation, taking into account their relative multiplicities. The resulting <*M*–O> – <*r*> relations

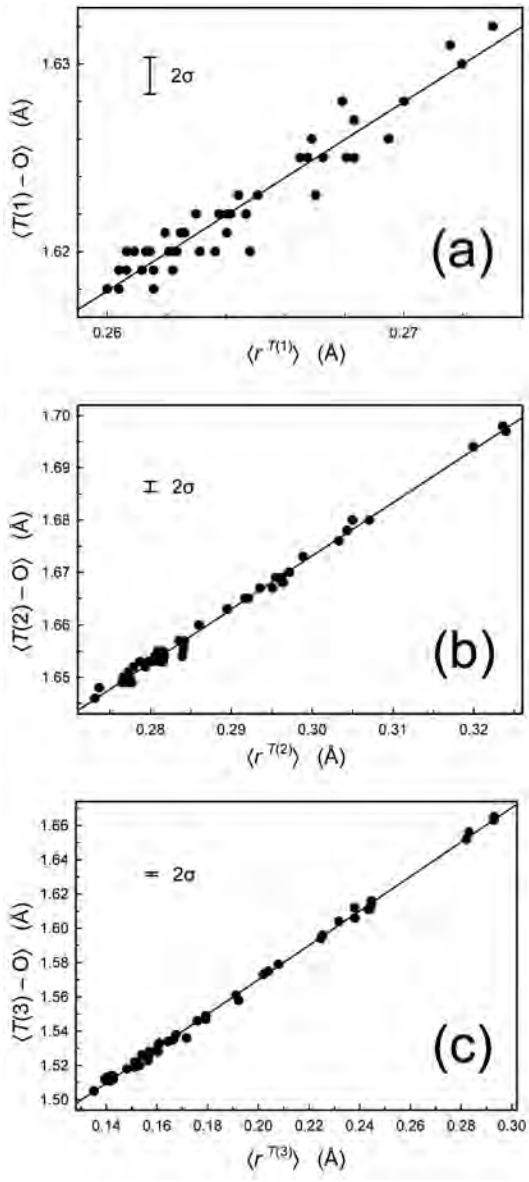

FIG. 6. Variation in <*T*–O> distance as a function of constituent-cation radius in kornerupine: (a) the *T*(1) site, (b) the *T*(2) site, (c) the *T*(3) site; regression lines are shown.

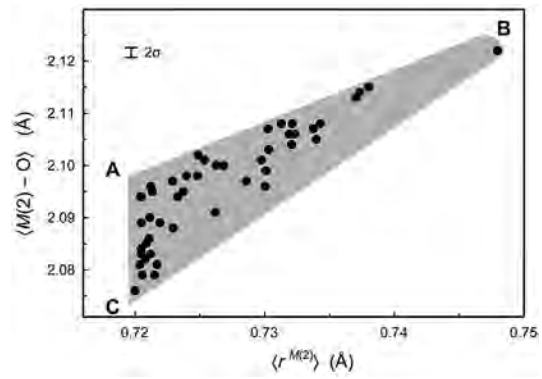

FIG. 7. Variation in <*M*(2)–O> distance as a function of constituent-cation radius in kornerupine; the dashed lines and grey shading define the field of data, and the letters A, B, C define the apices of the triangle for ease of reference in the text.

TABLE 7. KORNERUPINE: SITE SCATTERING AND SITE POPULATIONS

	K1	K2	K3	K5	K6	K7	K8	K9	K10	K11	K12	K13
X {*epfu*} [Mg]	5.25	4.99	4.45	5.01	6.11	5.81	7.54	6.18	6.14	4.26	4.68	4.85
X {*epfu*} [Fe]	5.10	4.81	4.31	4.84	5.91	5.62	7.23	5.96	5.90	4.14	4.51	4.68
Mg	0.142	0.217	0.091	0.130	0.117	0.207	0.107	0.131	0.103	0.071	0.283	0.314
Fe*	0.147	0.080	0.124	0.134	0.165	0.099	0.218	0.189	0.186	0.132	0.046	0.016
Na	0.010	0.000	0.025	0.010	0.010	0.000	0.000	0.012	0.000	0.012	0.000	0.000
Ca	0.000	0.000	0.000	0.000	0.000	0.000	0.000	0.000	0.000	0.000	0.011	0.000
□	0.701	0.703	0.760	0.726	0.708	0.694	0.675	0.668	0.711	0.785	0.660	0.670
M(1) {*epfu*}	26.80	25.68	31.62	26.97	31.11	25.90	30.44	26.58	30.38	33.91	24.73	24.56
Mg	1.800	1.880	1.456	1.788	1.492	1.864	1.540	1.816	1.544	1.292	1.948	1.960
Fe^{2+}	0.200	0.120	0.544	0.212	0.508	0.136	0.460	0.184	0.456	0.708	0.052	0.040
M(2) {*epfu*}	12.83	12.57	16.05	13.33	15.37	12.87	14.13	13.20	14.36	18.61	12.34	12.35
Mg	0.810	0.843	0.639	0.828	0.662	0.848	0.731	0.857	0.742	0.448	0.828	0.907
Al	0.141	0.125	0.077	0.083	0.105	0.097	0.126	0.062	0.096	0.086	0.159	0.073
Fe^{2+}	0.049	0.032	0.284	0.089	0.233	0.055	0.143	0.081	0.162	0.466	0.013	0.020
M(3) {*epfu*}	26.00	26.00	26.00	26.00	26.00	26.00	26.00	26.00	26.00	26.00	26.00	26.00
Al	1.926	1.932	1.984	1.974	1.960	1.958	1.944	1.972	1.952	1.986	1.910	1.968
Mg	0.074	0.068	0.016	0.026	0.040	0.042	0.056	0.028	0.048	0.014	0.090	0.032
M(4) {*epfu*}	26.63	26.62	27.68	25.68	27.88	26.12	28.36	26.27	27.59	25.98	26.03	25.56
Al	1.562	1.504	1.664	1.626	1.474	1.444	1.396	1.484	1.458	1.780	1.578	1.446
Mg	0.358	0.416	0.192	0.370	0.354	0.508	0.392	0.460	0.386	0.200	0.390	0.546
Fe^{3+}	0.068	0.080	0.144	0.004	0.172	0.048	0.212	0.056	0.144	0.000	0.032	0.008
Ti	0.012	0.000	0.000	0.000	0.000	0.000	0.000	0.000	0.012	0.020	0.000	0.000
Cr	0.000	0.000	0.000	0.000	0.000	0.000	0.000	0.000	0.000	0.000	0.000	0.000
V	0.000	0.000	0.000	0.000	0.000	0.000	0.000	0.000	0.000	0.000	0.000	0.000
M(5) {*epfu*}	26.00	26.00	26.00	26.00	26.00	26.00	26.00	26.00	26.00	26.00	26.00	26.00
Al	1.970	1.974	1.974	1.984	1.972	1.968	1.976	1.972	1.974	1.964	1.964	1.968
Mg	0.030	0.026	0.026	0.016	0.028	0.032	0.024	0.028	0.026	0.036	0.036	0.032
T(1) {*epfu*}	27.89	27.90	27.98	27.97	27.97	27.98	27.92	27.99	27.94	27.99	27.87	27.99
Si	1.888	1.900	1.982	1.966	1.970	1.976	1.922	1.994	1.942	1.994	1.872	1.990
Al	0.112	0.100	0.018	0.034	0.030	0.024	0.078	0.006	0.058	0.006	0.128	0.010
T(2) {*epfu*}	27.44	27.55	27.63	27.67	27.60	27.75	27.43	27.73	27.63	27.67	27.32	27.79
Si	1.442	1.546	1.628	1.674	1.600	1.746	1.428	1.732	1.634	1.670	1.318	1.790
Al	0.558	0.454	0.372	0.326	0.400	0.254	0.572	0.268	0.366	0.330	0.682	0.210
T(3) {*epfu*}	10.17	9.25	6.53	7.17	7.29	7.13	8.92	6.33	7.60	6.18	11.11	6.35
Si	0.402	0.343	0.094	0.155	0.177	0.148	0.340	0.084	0.204	0.057	0.481	0.103
Al	0.194	0.145	0.086	0.097	0.087	0.100	0.108	0.072	0.096	0.083	0.223	0.053
B	0.404	0.512	0.820	0.748	0.736	0.752	0.552	0.844	0.700	0.860	0.296	0.844
O(10) {*epfu*}	8.00	8.00	8.28	8.08	8.20	8.08	8.00	8.08	8.04	8.32	8.00	8.12
O	1.00	1.00	0.72	0.92	0.80	0.92	1.00	0.92	0.96	0.68	1.00	0.88
F	0.00	0.00	0.28	0.08	0.20	0.08	0.00	0.08	0.04	0.32	0.00	0.12

Site-scattering values are expressed in {epfu}; the e.s.d. is ~0.1 electrons; site populations are quoted in *apfu*. * Fe = (Fe^{2+} + Mn^{2+}).

are shown in Figure 9 and listed in Table 8. No data lie more than 3σ from the least-squares fits to the data, indicating that variations in the r^2 values represent only the magnitude of the standard deviations of the data relative to the total variation in the data (*i.e.*, <*M*–O>). The slopes for the *M*(2) and *M*(3) sites are 0.97 and 0.93, respectively, close to the ideal value of 1.0. The slopes for the *M*(4) and *M*(5) sites are 0.78 and 0.84, respectively. The latter value is not well constrained (Fig. 9d), whereas the former values shows significant deviation from 1.0. This type of situation, in which most sites closely follow a hard-sphere model but some deviate significantly, occurs in other common minerals (*e.g.*, monoclinic amphiboles: Hawthorne 1983).

The M(1) site: The relation between <*M*(1)–O> and <$r^{M(1)}$> [corrected for variations in anion composition

TABLE 7 (cont'd). KORNERUPINE: SITE SCATTERING AND SITE POPULATIONS

	K14	K15	K16	K17	K18	K19	K20	K21	K22	K23	K24	K25
X {*epfu*} [Mg]	3.89	6.78	3.65	5.79	5.62	3.84	3.31	5.38	4.13	3.22	3.74	5.97
X {*epfu*} [Fe]	3.74	6.54	3.54	5.60	5.43	3.73	3.18	5.20	3.98	3.12	3.61	5.78
Mg	0.120	0.113	0.083	0.113	0.151	0.119	0.104	0.105	0.246	0.282	0.117	0.095
Fe*	0.098	0.216	0.109	0.165	0.142	0.075	0.064	0.152	0.050	0.000	0.063	0.177
Na	0.000	0.027	0.000	0.029	0.000	0.022	0.017	0.000	0.000	0.000	0.026	0.015
Ca	0.000	0.000	0.000	0.000	0.000	0.000	0.000	0.000	0.000	0.000	0.000	0.000
□	0.782	0.644	0.808	0.693	0.707	0.784	0.815	0.743	0.704	0.718	0.794	0.713
M(1) {*epfu*}	31.67	29.43	33.74	30.16	28.82	28.42	31.28	30.05	24.84	24.45	28.65	29.94
Mg	1.452	1.612	1.304	1.560	1.656	1.684	1.480	1.568	1.940	1.968	1.668	1.576
Fe^{2+}	0.548	0.388	0.696	0.440	0.344	0.316	0.520	0.432	0.060	0.032	0.332	0.424
M(2) {*epfu*}	14.97	14.46	16.11	14.51	13.69	14.70	16.28	13.59	12.33	12.20	14.91	15.42
Mg	0.699	0.723	0.647	0.727	0.791	0.742	0.624	0.751	0.851	0.902	0.715	0.674
Al	0.096	0.109	0.064	0.101	0.095	0.070	0.076	0.146	0.135	0.090	0.083	0.088
Fe^{2+}	0.205	0.168	0.289	0.172	0.114	0.188	0.300	0.103	0.014	0.008	0.202	0.238
M(3) {*epfu*}	26.00	26.00	26.00	26.00	26.00	26.00	26.00	26.00	26.00	26.00	26.00	26.00
Al	1.978	1.930	1.988	1.954	1.960	1.980	1.990	1.920	1.914	1.966	1.966	1.980
Mg	0.022	0.070	0.012	0.046	0.040	0.020	0.010	0.080	0.086	0.034	0.034	0.020
M(4) {*epfu*}	27.89	30.15	26.68	29.86	27.92	26.41	26.32	27.94	25.73	25.97	26.20	28.46
Al	1.532	1.142	1.720	1.266	1.404	1.674	1.756	1.540	1.622	1.588	1.700	1.366
Mg	0.296	0.496	0.206	0.406	0.416	0.264	0.194	0.284	0.370	0.376	0.254	0.408
Fe^{3+}	0.160	0.348	0.056	0.328	0.180	0.020	0.008	0.160	0.008	0.000	0.000	0.208
Ti	0.012	0.014	0.018	0.000	0.000	0.018	0.020	0.016	0.000	0.016	0.020	0.018
Cr	0.000	0.000	0.000	0.000	0.000	0.014	0.012	0.000	0.000	0.000	0.014	0.000
V	0.000	0.000	0.000	0.000	0.000	0.010	0.010	0.000	0.000	0.020	0.012	0.000
M(5) {*epfu*}	26.00	26.00	26.00	26.00	26.00	26.00	26.00	26.00	26.00	26.00	26.00	26.00
Al	1.988	1.972	1.988	1.976	1.972	1.980	1.980	1.974	1.968	1.976	1.978	1.970
Mg	0.012	0.028	0.012	0.024	0.028	0.020	0.020	0.026	0.032	0.024	0.022	0.030
T(1) {*epfu*}	27.98	27.93	28.00	27.96	27.95	27.99	28.00	27.89	27.90	27.97	27.99	27.99
Si	1.978	1.928	2.000	1.960	1.954	1.994	2.000	1.894	1.896	1.966	1.990	1.986
Al	0.022	0.072	0.000	0.040	0.046	0.006	0.000	0.106	0.104	0.034	0.010	0.014
T(2) {*epfu*}	27.64	27.67	27.70	27.67	27.68	27.73	27.71	27.40	27.51	27.69	27.74	27.72
Si	1.638	1.666	1.696	1.668	1.678	1.734	1.712	1.402	1.512	1.688	1.744	1.724
Al	0.362	0.334	0.304	0.332	0.322	0.266	0.288	0.598	0.488	0.312	0.256	0.276
T(3) {*epfu*}	7.12	7.49	6.19	7.01	7.06	6.33	6.11	10.44	10.00	7.34	6.63	6.30
Si	0.165	0.186	0.068	0.152	0.170	0.085	0.058	0.416	0.361	0.167	0.096	0.082
Al	0.079	0.102	0.072	0.080	0.066	0.071	0.074	0.212	0.219	0.105	0.096	0.070
B	0.756	0.712	0.860	0.768	0.764	0.844	0.868	0.372	0.420	0.728	0.808	0.848
O(10) {*epfu*}	8.08	8.24	8.16	8.16	8.04	8.36	8.32	8.16	8.00	8.08	8.36	8.32
O	0.92	0.76	0.84	0.84	0.96	0.64	0.68	0.84	1.00	0.92	0.64	0.68
F	0.08	0.24	0.16	0.16	0.04	0.36	0.32	0.16	0.00	0.08	0.36	0.32

Site-scattering values are expressed in {epfu}; the e.s.d. is ~0.1 electrons; site populations are quoted in *apfu*. * Fe = (Fe^{2+} + Mn^{2+}).

at O(10)] is quite non-linear if the refined site-scattering is expressed as Mg and Fe^{2+} (Fig. 10a). In Figure 10a, the B content of each crystal is indicated qualitatively by the types of symbols used. The sample group with the largest content of boron (black circles) shows a linear relation between <*M*(1)–O> and $<r^{M(1)}>$ (the broken line AB with a slope of ~0.7). Samples with progressively less B (dotted circles and hollow circles, respectively) show progressive deviation from the line AB. Multiple linear-regression with <*M*(1)–O> as the dependent variable and $<r^{M(1)}>$ and B content as independent variables gives a much improved fit (r^2 = 0.86, Table 8). Figure 10b compares the observed and calculated <*M*(1)–O> values; the data lie within three standard deviations of the 1:1 relation.

TABLE 7 (cont'd). KORNERUPINE: SITE SCATTERING AND SITE POPULATIONS

	K26	K27	K28	K29	K30	K31	K32	K33	K34	K35	K36	K38
X {*epfu*} [Mg]	7.10	6.05	6.29	6.28	3.70	3.89	5.57	5.34	4.17	5.79	6.67	5.28
X {*epfu*} [Fe]	6.84	5.82	6.06	6.06	3.57	3.74	5.38	5.19	4.04	5.58	6.45	5.10
Mg	0.073	0.131	0.184	0.091	0.292	0.284	0.272	0.117	0.123	0.184	0.163	0.250
Fe*	0.231	0.177	0.130	0.182	0.008	0.022	0.076	0.136	0.079	0.142	0.199	0.100
Na	0.017	0.000	0.000	0.017	0.000	0.000	0.000	0.032	0.034	0.000	0.000	0.000
Ca	0.000	0.000	0.000	0.000	0.012	0.000	0.000	0.000	0.000	0.011	0.000	0.000
□	0.679	0.692	0.686	0.710	0.688	0.694	0.652	0.715	0.764	0.663	0.638	0.650
M(1) {*epfu*}	29.71	28.48	26.35	30.55	24.22	24.56	25.85	28.98	27.64	25.62	25.34	24.90
Mg	1.592	1.680	1.832	1.532	1.984	1.960	1.868	1.644	1.740	1.884	1.904	1.936
Fe^{2+}	0.408	0.320	0.168	0.468	0.016	0.040	0.132	0.356	0.260	0.116	0.096	0.064
M(2) {*epfu*}	14.46	13.55	13.01	14.91	12.18	12.22	12.75	15.31	14.49	12.54	12.57	12.40
Mg	0.712	0.806	0.848	0.707	0.824	0.854	0.872	0.670	0.735	0.786	0.798	0.832
Al	0.121	0.090	0.086	0.092	0.176	0.140	0.080	0.101	0.094	0.189	0.174	0.150
Fe^{2+}	0.167	0.104	0.066	0.201	0.000	0.006	0.048	0.229	0.171	0.025	0.028	0.018
M(3) {*epfu*}	26.00	26.00	26.00	26.00	26.00	26.00	26.00	26.00	26.00	26.00	26.00	26.00
Al	1.926	1.970	1.966	1.964	1.884	1.910	1.960	1.960	1.960	1.888	1.892	1.900
Mg	0.074	0.030	0.034	0.036	0.116	0.090	0.040	0.040	0.040	0.112	0.108	0.100
M(4) {*epfu*}	28.72	27.47	26.40	26.79	25.67	25.77	25.72	27.74	26.24	26.58	27.68	26.70
Al	1.386	1.402	1.444	1.610	1.672	1.716	1.500	1.592	1.628	1.678	1.542	1.522
Mg	0.370	0.450	0.488	0.306	0.328	0.280	0.484	0.248	0.316	0.254	0.302	0.390
Fe^{3+}	0.224	0.148	0.068	0.084	0.000	0.004	0.016	0.136	0.000	0.056	0.144	0.060
Ti	0.020	0.000	0.000	0.000	0.000	0.000	0.000	0.024	0.020	0.012	0.012	0.000
Cr	0.000	0.000	0.000	0.000	0.000	0.000	0.000	0.000	0.020	0.000	0.000	0.028
V	0.000	0.000	0.000	0.000	0.000	0.000	0.000	0.000	0.016	0.000	0.000	0.000
M(5) {*epfu*}	26.00	26.00	26.00	26.00	26.00	26.00	26.00	26.00	26.00	26.00	26.00	26.00
Al	1.968	1.970	1.976	1.974	1.928	1.974	1.960	1.982	1.970	1.920	1.924	1.964
Mg	0.032	0.030	0.024	0.026	0.072	0.026	0.040	0.018	0.030	0.080	0.076	0.036
T(1) {*epfu*}	27.93	27.96	27.96	27.94	27.85	27.89	27.95	27.94	27.98	27.80	27.82	27.88
Si	1.932	1.962	1.964	1.938	1.846	1.888	1.952	1.936	1.980	1.800	1.822	1.878
Al	0.068	0.038	0.036	0.062	0.154	0.112	0.048	0.064	0.020	0.200	0.178	0.122
T(2) {*epfu*}	27.45	27.68	27.70	27.51	27.28	27.33	27.74	27.51	27.73	27.08	27.02	27.31
Si	1.454	1.684	1.702	1.508	1.276	1.334	1.736	1.506	1.734	1.078	1.022	1.308
Al	0.546	0.316	0.298	0.492	0.724	0.666	0.264	0.494	0.266	0.922	0.978	0.692
T(3) {*epfu*}	9.23	7.08	7.08	8.15	12.69	10.87	6.63	8.00	7.01	13.54	13.38	10.96
Si	0.329	0.155	0.157	0.268	0.589	0.429	0.096	0.217	0.119	0.703	0.727	0.489
Al	0.159	0.085	0.083	0.092	0.299	0.251	0.096	0.131	0.117	0.277	0.229	0.195
B	0.512	0.760	0.760	0.640	0.112	0.320	0.808	0.652	0.764	0.020	0.044	0.316
O(10) {*epfu*}	8.16	8.04	8.12	8.12	8.00	8.00	8.00	8.48	8.44	8.00	8.04	8.00
O	0.84	0.96	0.88	0.88	1.00	1.00	1.00	0.52	0.56	1.00	0.96	1.00
F	0.16	0.04	0.12	0.12	0.00	0.00	0.00	0.48	0.44	0.00	0.04	0.00

Site-scattering values are expressed in {epfu}; the e.s.d. is ~0.1 electrons; site populations are quoted in *apfu*. * Fe = (Fe^{2+} + Mn^{2+}).

The non-linearity in Figure 10a cannot be attributed to incorporation of a larger cation at *M*(1), as the chemical compositions (Table 4) are not in accord with this possibility. Two *M*(1) octahedra link through the O(10) anion, and the O(5)–O(7) edge is shared between the *M*(1) octahedron and the *T*(2) tetrahedron. The chemical variation in the *T*(2)–*T*(3)–*T*(2) tetrahedron trimer is thus closely tied to the *M*(1) site *via* the shared O(5)–O(7) edges (see later discussion). Thus we propose that variation of B, Al and Si in the *T*(2)–*T*(3)–*T*(2) trimer induces a steric response in the *M*(1) octahedron.

TABLE 7 (cont'd). KORNERUPINE: SITE SCATTERING AND SITE POPULATIONS

	K39	K40	K41	K42	K43	K45	K46	K47	K49	K50	K52
X {*epfu*} [Mg]	4.90	4.22	5.71	5.95	3.02	5.73	3.61	3.56	6.58	4.22	4.03
X {*epfu*} [Fe]	4.71	4.06	5.54	5.73	2.89	5.51	3.48	3.45	6.37	4.06	3.87
Mg	0.245	0.309	0.352	0.143	0.281	0.210	0.340	0.343	0.276	0.279	0.393
Fe*	0.095	0.029	0.039	0.133	0.000	0.093	0.000	0.000	0.111	0.029	0.000
Na	0.000	0.000	0.000	0.017	0.010	0.019	0.000	0.000	0.000	0.000	0.000
Ca	0.000	0.012	0.012	0.000	0.000	0.000	0.010	0.010	0.000	0.000	0.000
□	0.660	0.650	0.597	0.707	0.719	0.678	0.650	0.647	0.613	0.692	0.607
M(1) {*epfu*}	25.01	24.17	24.78	29.49	24.50	26.46	24.28	24.34	25.90	24.84	24.22
Mg	1.928	1.988	1.944	1.608	1.964	1.824	1.980	1.976	1.864	1.940	1.984
Fe^{2+}	0.072	0.012	0.056	0.392	0.036	0.176	0.020	0.024	0.136	0.060	0.016
M(2) {*epfu*}	12.40	12.30	12.38	14.85	12.20	13.20	12.27	12.26	12.95	12.43	12.23
Mg	0.850	0.817	0.909	0.723	0.890	0.840	0.835	0.841	0.854	0.831	0.872
Al	0.131	0.174	0.069	0.079	0.103	0.080	0.157	0.151	0.084	0.149	0.120
Fe^{2+}	0.019	0.009	0.022	0.198	0.007	0.080	0.008	0.008	0.062	0.020	0.008
M(3) {*epfu*}	26.00	26.00	26.00	26.00	26.00	26.00	26.00	26.00	26.00	26.00	26.00
Al	1.928	1.898	1.968	1.974	1.958	1.966	1.904	1.904	1.950	1.904	1.946
Mg	0.072	0.102	0.032	0.026	0.042	0.034	0.096	0.096	0.050	0.096	0.054
M(4) {*epfu*}	26.21	26.00	25.94	26.18	25.85	25.88	26.03	25.98	26.38	25.91	25.62
Al	1.518	1.714	1.326	1.604	1.636	1.546	1.574	1.576	1.428	1.630	1.454
Mg	0.430	0.262	0.630	0.344	0.344	0.430	0.386	0.388	0.504	0.350	0.534
Fe^{3+}	0.036	0.012	0.044	0.012	0.004	0.024	0.000	0.000	0.068	0.020	0.012
Ti	0.000	0.012	0.000	0.028	0.016	0.000	0.014	0.012	0.000	0.000	0.000
Cr	0.016	0.000	0.000	0.000	0.000	0.000	0.026	0.024	0.000	0.000	0.000
V	0.000	0.000	0.000	0.012	0.000	0.000	0.000	0.000	0.000	0.000	0.000
M(5) {*epfu*}	26.00	26.00	26.00	26.00	26.00	26.00	26.00	26.00	26.00	26.00	26.00
Al	1.960	1.932	1.946	1.964	1.980	1.966	1.958	1.958	1.972	1.968	1.978
Mg	0.040	0.068	0.054	0.036	0.020	0.034	0.042	0.042	0.028	0.032	0.022
T(1) {*epfu*}	27.90	27.82	27.97	27.98	27.94	27.94	27.85	27.88	27.93	27.87	27.89
Si	1.900	1.816	1.968	1.976	1.938	1.944	1.854	1.876	1.926	1.872	1.892
Al	0.100	0.184	0.032	0.024	0.062	0.056	0.146	0.124	0.074	0.128	0.108
T(2) {*epfu*}	27.48	27.02	27.80	27.67	27.63	27.73	27.44	27.46	27.63	27.44	27.63
Si	1.484	1.016	1.798	1.668	1.630	1.728	1.440	1.460	1.632	1.442	1.630
Al	0.516	0.984	0.202	0.332	0.370	0.272	0.560	0.540	0.368	0.558	0.370
T(3) {*epfu*}	9.49	13.58	6.03	6.66	7.92	6.92	10.83	10.51	7.57	10.68	8.43
Si	0.358	0.712	0.065	0.090	0.200	0.125	0.426	0.393	0.172	0.395	0.229
Al	0.158	0.272	0.055	0.106	0.140	0.099	0.250	0.247	0.128	0.265	0.171
B	0.484	0.016	0.880	0.804	0.660	0.776	0.324	0.360	0.700	0.340	0.600
O(10) {*epfu*}	8.00	8.00	8.04	8.24	8.00	8.12	8.00	8.00	8.08	8.00	8.00
O	1.00	1.00	0.96	0.76	1.00	0.88	1.00	1.00	0.92	1.00	1.00
F	0.00	0.00	0.04	0.24	0.00	0.12	0.00	0.00	0.08	0.00	0.00

Site-scattering values are expressed in {epfu}; the e.s.d. is ~0.1 electrons; site populations are quoted in *apfu*. * Fe = (Fe^{2+} + Mn^{2+}).

Assessment of final M(3) and M(5) site-populations

Inspection of Table 7 shows that the *M*(3) and *M*(5) sites are occupied predominantly by Al, with only minor amounts (<0.12 and 0.08 *apfu*, respectively) of Mg. Let us briefly examine the criteria that pertain to these assignments, as they do differ from previous assigned site-populations (Table 1).

If the <*M*(3)–O> distances are ordered in terms of increasing value (Fig. 8), the <*M*(5)–O> distances show a similar pattern of order. As noted above, this could be due to (1) correlated structural strain, or (2) incorporation of an additional constituent with a larger radius and a similar scattering-power (*i.e.*, Mg). If sufficient Mg is assigned to *M*(3) and *M*(5) to attain linearity (Figs. 9b, d), an equivalent amount of Mg has

to be taken from the assigned site-populations for any or all of the *M*(1), *M*(2) and *M*(4) sites. Pertinent to this issue is that the initially assigned site-populations at *M*(2) produced a relation with considerable systematic scatter (Fig. 7). Removal of sufficient Mg from *M*(2) to produce linearity in plots of bond length *versus* constituent radius for the *M*(3) and *M*(5) sites (Figs. 9b, d) produces linearity in the analogous plot for the *M*(2) site (*cf.* Fig. 7 and Fig. 9a). This seems an unlikely result if the incorporation of Mg into the *M*(3) and *M*(5) sites were incorrect. Thus we conclude that the site populations shown in Table 7 are correct.

Final Assignment of Site Populations: The X Site

The *X* site is the most difficult one to deal with, as it is occupied by Mg, Fe^{2+}, Mn^{2+}, Ca, Na and □ (vacancy). Values for Mn^{2+}, Ca and Na were assigned from the unit formulae; this leaves Mg, Fe^{2+} and □ to be assigned in the refinement process. The Mg and Fe^{2+} contents remaining after assignment to the *M* sites are assigned to the *X* site, and the resulting □ is calculated as $1.0 - {}^{X}Mg - {}^{X}Fe^{2+} - Mn^{2+} - Na - Ca$. The <*X*–O> distances are shown as a function of the □ content in Figure 11a. The data define a triangle, converging with increasing □ content to a point at <*X*–O> ≈ 2.415 Å and ${}^{X}□ \approx 0.83$. It seems reasonable to propose that a completely vacant *X* site will have <*X*–O> = 2.415 Å. Thus we may calculate a radius for ${}^{X}□$: 2.415 – 1.37 = 1.045 Å, where 1.37 Å is the appropriate radius for an O atom. This allows us to plot <*X*–O> *versus* $\langle r^{X} \rangle$ [corrected for variations in F ⇌ OH substitution at O(10); Fig. 11b]. In Figure 11b, the B content of each crystal is indicated qualitatively by the symbols used, suggesting that <*X*–O> also correlates with the B content of the crystal. Multiple regression with <*X*–O> as the dependent variable and $\langle r^{X} \rangle$, F and B as independent variables gave an r^2 value of 0.897; in Figure 11c, we compare the corresponding observed and calculated <*X*–O> values.

Thus far, the cations assigned to *X* come from the unit formulae calculated from the chemical compositions and the results of a site-scattering refinement of the *T* and *M* sites. These values are reasonably compatible with the observed <*X*–O> distances. How do they compare with the refined site-scattering values at the *X* site? The latter were determined as follows: (1) Na and Ca occupancies were assigned from the unit formula, (2) the occupancy of Mg was refined [with no Fe* (≡ Fe + Mn) present], and (3) the occupancy of Fe was refined [with no Mg present].

The total scattering at the *X* site (in *epfu*) is slightly different for (2) and (3), respectively, as the *shapes* of the scattering curves for Mg and Fe are slightly different. Figure 11d shows the total scattering as a function of the corresponding values calculated from the unit formula; the values agree to within one-half an electron [the bars in Fig. 11d represent the range of values from procedures (2) and (3) above, together with the standard deviation of each of these determinations], indicating that the assigned site-populations are in accord with the site-scattering refinement.

Final assigned site-populations and associated regression models are given in Tables 7 and 8, and a graphical summary of the compositional ranges for each of the nine distinct cation-sites is shown in Figure 12.

Cation Order at the *T* Sites

The *T*(1), *T*(2) and *T*(3) tetrahedra polymerize to form two distinct clusters, a $[T_2O_7]$ dimer and a $[T_3O_{10}]$ trimer.

The T(1)–T(1)' dimer

Up to 0.200 Al *apfu* was assigned to the *T*(1) site (Table 7). The two criteria supporting this assignment are: (1) <*T*(1)–O> variation of 0.014 Å (*i.e.*, 1.618 → 1.632 Å); (2) improved linearity between <*T*–O> distances and constituent-cation radii at the *T*(2) and *T*(3) sites. It is well known that the average Al content of a tetrahedron affects <*T*–O> distances (Smith 1954,

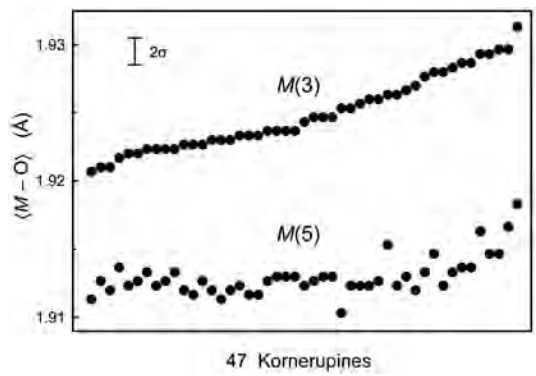

FIG. 8. Variation in <*M*(3)–O> and <*M*(5)–O> distances in kornerupine; the data are organized in terms of increasing <*M*(3)–O> distance toward the right side of the figure.

TABLE 8. REGRESSION EQUATIONS TO PREDICT MEAN BOND-LENGTHS USING VARIOUS CHEMICAL PARAMETERS FOR THE NINE CRYSTALLOGRAPHIC SITES IN KORNERUPINE

<*T*(1)–O>	= 1.3560 + 1.0074 $\langle r^{T(1)} \rangle$	r^2 = 0.927	Fig. 6a
<*T*(2)–O>	= 1.3679 + 1.0176 $\langle r^{T(2)} \rangle$	r^2 = 0.994	Fig. 6b
<*T*(3)–O>	= 1.3692 + 1.0039 $\langle r^{T(3)} \rangle$	r^2 = 0.998	Fig. 6c
<*M*(1)–O>	= 1.6813 + 0.6087 $\langle r^{M(1)} \rangle$ – 0.0094 B	r^2 = 0.855	Fig. 10b
<*M*(2)–O>	= 1.4098 + 0.9722 $\langle r^{M(2)} \rangle$	r^2 = 0.976	Fig. 9a
<*M*(3)–O>	= 1.4241 + 0.9276 $\langle r^{M(3)} \rangle$	r^2 = 0.895	Fig. 9b
<*M*(4)–O>	= 1.5103 + 0.7802 $\langle r^{M(4)} \rangle$	r^2 = 0.993	Fig. 9c
<*M*(5)–O>	= 1.4631 + 0.8363 $\langle r^{M(5)} \rangle$	r^2 = 0.626	Fig. 9d
<*X*–O>	= 1.8512 + 0.5725 $\langle r^{X} \rangle$ – 0.0279 B + 0.0240 F	r^2 = 0.897	Fig. 11c

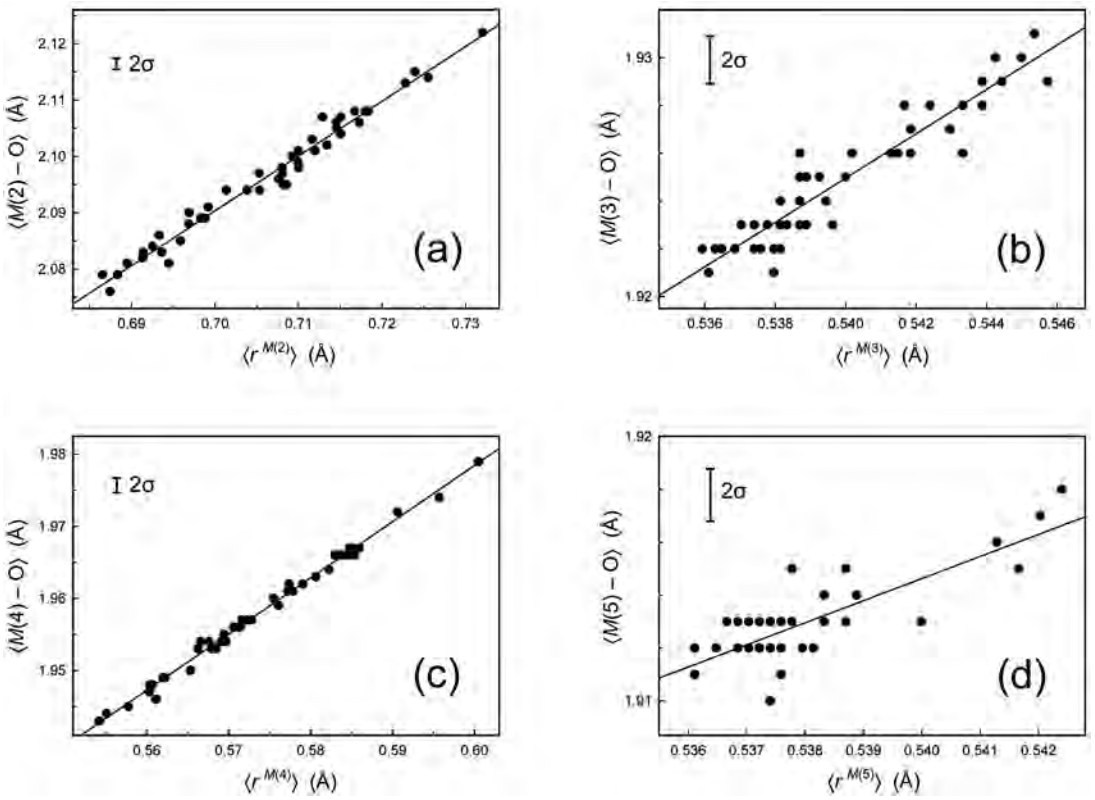

FIG. 9. Variation in <*M*–O> distance as a function of constituent-cation radius in kornerupine: (a) the *M*(2) site, (b) the *M*(3) site, (c) the *M*(4) site, and (d) the *M*(5) site; regression lines are shown.

Smith & Bailey 1963). However, the bond lengths are also affected by geometrical changes in the local environment. A useful parameter in this regard is the *T*–O(br: bridging)–*T* angle or, more specifically, 1/(1 – sec*TOT*) (Swanson 1980, Swanson *et al.* 1980). This quantity is referred to as f_s(O), the fractional *s*-character of the bond involving the bridging O atom. There are slightly different minimum-energy angles for *Si*–O–*Si* and *Si*–O–*Al* configurations (Geisinger *et al.* 1985). Therefore, f_s values for O(9) as calculated from *T*(1)–O(9)–*T*(1) angles should contain information on the probability of Al ordering at *T*(1). To test this hypothesis, <*T*(1)–O> distances are plotted against f_s values for O(9) in Figure 13. The solid line is taken from Geisinger *et al.* (1985), who used <*Si*–O> and *Si*–O–*Si* values from well-ordered framework silicates to develop the line *via* regression analysis. The line is shifted upward (0.014 Å) relative to that of Geisinger *et al.* (1985), so that it would pass through the lower data in Figure 13. The slope of the line is both shallow and negative (–0.229), indicating that, as *Si*–O–*Si* angles increase, there is a decrease in <*T*(1)–O> distance. A similar trend (slope = –0.312) was found by Geisinger *et al.* (1985) for *Al*–O–*Si* angles (the trend is displaced vertically by +0.13 Å along the <*T*(1)–O> axis and plots off Fig. 13). Data above the solid line correspond to progressively more assigned Al [this reflects the fact that Al populations were extrapolated directly from <*T*(1)–O> distances]. However, the data plotting near a *T*(1)–O(9)–*T*(1) angle of ~148.8° [f_sO(9) ≈ 0.461] span an appreciable range in <*T*–O>, and a rather limited range in f_sO(9). The data points with greater assigned Al deviate more substantially from the line of Geisinger *et al.* (1985) for (*Si*–O–*Si*). This deviation toward greater <*T*–O> distance for a given *T*–O–*T* angle is consistent with Al at the *T*(1) site. The strength of the hydrogen bond to O(9) is very weak, and its potential perturbing effect on the *T*–O–*T* angle can probably be disregarded.

T(2)–T(3)–T(2) trimer

The molecular-orbital study of Geisinger *et al.* (1985) also involved calculation of minimum-energy

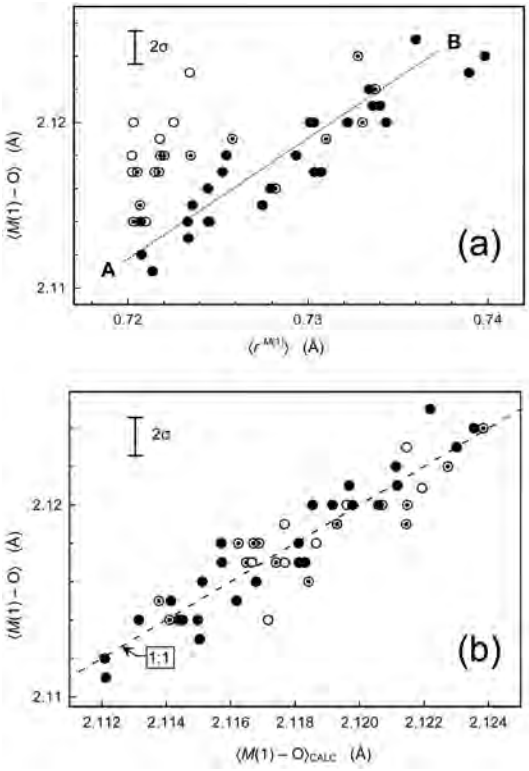

FIG. 10. Variation in <*M*(1)–O> distance in kornerupine: (a) as a function of constituent-cation radius; the broken line indicates a linear relation through data for crystals of high content of boron (black circles); (b) observed *versus* calculated <*M*(1)–O> distance; the dashed line shows the 1:1 relation. Black circles: > 0.67 B; circle with enclosed dot: 0.33 ≤ B ≤ 0.67 B; open circles: B < 0.33 *apfu*.

angles for the *Si*–O–*B* configuration (the minimum-energy angle for a [2]-coordinated bridging atom of oxygen is equal to 125°). In kornerupine, the bridging O(7) atom is also linked to the *M*(1) cation in addition to *T*(2) and *T*(3), and is therefore [3]-coordinated. In this case, the *T*–O–*T* angle should be significantly smaller and show a smaller range than that for a [2]-coordinated bridging anion (Geisinger *et al*. 1985). The range in observed *T*(2)–O(7)–*T*(3) angles (Fig. 14a) is only 2.8°, and agrees with that predicted by Geisinger *et al*. (*i.e.*, <125°). A striking feature of Figure 14a is the uniform positive correlation between increasing B content and increasing *T*(2)–O(7)–*T*(3) angle, from ~0.0 to 0.7 B *apfu*. As the B population increases at *T*(3), $^{T(2)}$Si–O–$^{T(3)}$B (and possibly $^{T(2)}$Al–O–$^{T(3)}$B) configurations must increase in frequency. The minimum-energy calculations of Geisinger *et al*. (1985) predict the opposite trend, *i.e.*, decreasing *T*(2)–O(7)–*T*(3) angles with increasing B. The local environment about the *T*(2)–*T*(3)–*T*(2) trimer is clearly exerting an influence on the observed *T*(2)–O(7)–*T*(3) angle that is greater than the driving force associated with attainment of the predicted minimum-energy angle. The linkage of the *T*(2)–*T*(3)–*T*(2) trimer to the neighboring polyhedra (Fig. 15) shows that the O(6)–O(8) edge of the *M*(5) octahedron and the O(5)–O(7) edge of the *M*(1) octahedron constrain the flexure of the tetrahedron trimer in the (001) plane. Within the kornerupine structure, the *M*(5) octahedron is the most inflexible element of the polyhedra in terms of both bond length and site-population variation (Tables 6, 7). The O(6)–O(8) edge of the *M*(5) octahedron has a maximum variation in length of only 0.046 Å. The maximum variation in the length of the O(5)–O(7) polyhedron edge that is shared between *T*(2) and *M*(1) (Fig. 15) is only 0.029 Å.

How are the <*T*(3)–O> distances able to span 0.16 Å while constrained by these relatively rigid neighbors? The answer lies in coupled shrinkage of the *T*(3) tetrahedron and rotation of the *T*(2) tetrahedron. In Figure 15, the light grey tetrahedra are drawn using coordinates from K35 (low B); corresponding *T*(2) and *T*(3) cation positions are shown as light grey circles. The dark grey tetrahedra are drawn using coordinates from K41 (high B); corresponding *T*(2) and *T*(3) cation positions are shown as black circles. The *T*(2), *T*(3), O(5), O(7), *M*(1), *M*(4), O(1), O(10) sites and their symmetry-related sites across the (100) mirror ($x = 0$) are situated on the (001) mirror ($z = ¼$) [*i.e.*, in the plane of the page]. The *M*(3), *M*(5), O(6) and O(8) sites lie above and below the (001) mirror. Visual inspection of the O(6)–O(8) and O(5)–O(7) edges at low- and high-B values shows that only minor adjustments in length occur. In this projection, the largest displacements involve the O(5), O(7), *T*(2) and *T*(3) sites; with increasing B, O(8) is stationary and O(7) migrates toward the central *T*(3) cation. With the resulting shrinkage of the *T*(3) tetrahedron, the *T*(3) atom moves toward the O(8)–O(8)' edge to maintain a central position within the tetrahedron. With negligible change in the O(6) position and O(5)–O(7) edge-length, the *T*(2) tetrahedron rotates about the O(6) position in tandem with the shrinking *T*(3) tetrahedron. Through this rotation, the size of the *T*(2) tetrahedron decreases from 1.694 (K35) to 1.646 Å (K41) (Table 6).

The most important neighboring feature coupled to this flexure of the *T*(2)–*T*(3)–*T*(2) tetrahedron trimer is the rotation of the O(5)–O(7) edge. Tied to this rotation are significant geometric adjustments to the *M*(1) and *M*(4) octahedra (Fig. 15). With increasing B, the *M*(1) and *M*(1)' octahedra can easily adjust *via* flexure at the corner-sharing anion O(10). Necessary adjustments along O(1)–O(5) are more constraining because this edge is shared between the *M*(1) and *M*(4) octahedra. This accommodation by the *M*(1) and *M*(4) octahedra to the changing position of the O(5)–O(7) edge relates to two previous observations: (1) proposed neighboring steric influences at *M*(1) as a function of B content at

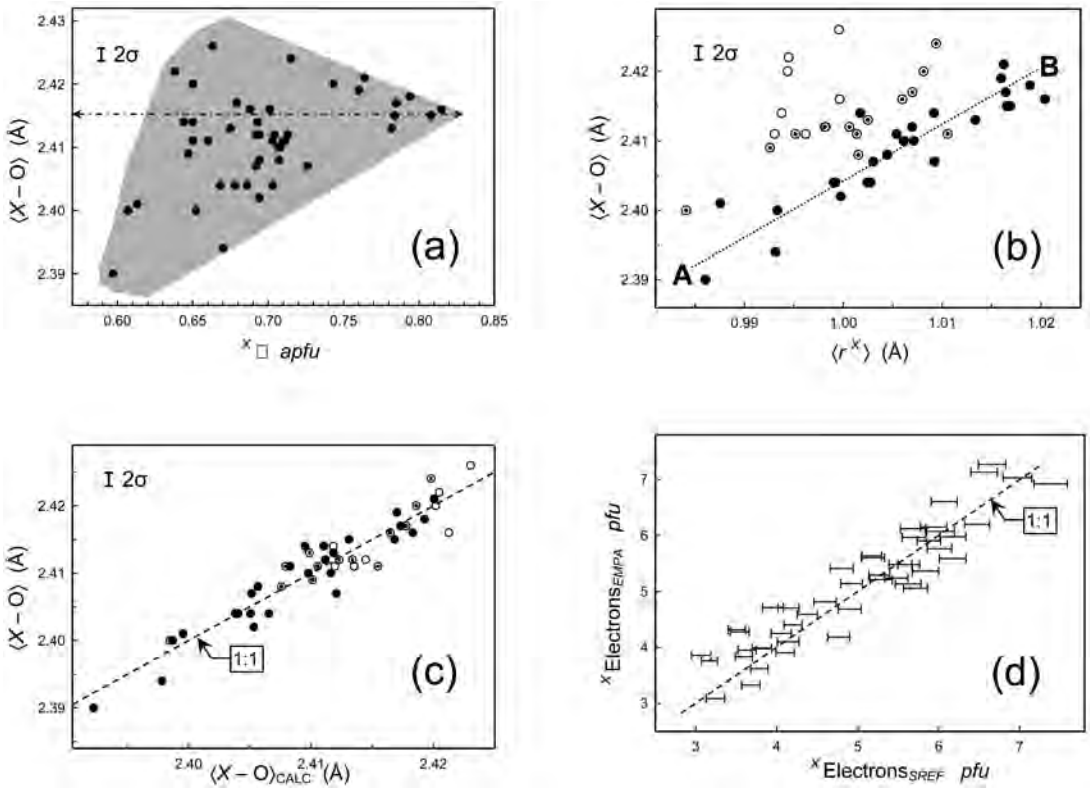

FIG. 11. Stereochemical variations at the *X* site in kornerupine: (a) <*X*–O> distance as a function of $^{X}\square$ (vacancy); the grey shading indicates the limits of distribution of the data, converging at <*X*–O> ≈ 2.415 Å, $^{X}\square$ = 0.83 *apfu*; (b) the <*X*–O> distance as a function of constituent-cation radius; the broken line indicates a linear relation through data for crystals of high content of B (black circles); legend for symbols as in Figure 10; (c) <*X*–O> observed *versus* <*X*–O> calculated; the line shows the 1:1 relation; (d) total number of electrons at the *X* site as calculated from the assigned site-populations (see text) *versus* the refined site-scattering values at the *X* site (see text for meaning of "error" bars); the dashed line shows the 1:1 relation.

T(3) that perturb the <*M*(1)–O> *versus* $<r^{M(1)}>$ relation; (2) the low slope (0.78) of the <*M*(4)–O> *versus* $<r^{M(4)}>$ relation. The first observation gains further credence from inspection of Figure 15: the low slope of the <*M*(4)–O> *versus* $<r^{\overline{M(4)}}>$ relation is complementary in helping maintain the incident bond-valence at the changing O(5) position.

An interesting feature of Figure 14a is the larger range of *T*(2)–O(7)–*T*(3) angles at greater B content (B > 0.7 *apfu*): at ~0.8 to 0.9 B, angles from 123.8 to 124.5° are observed. These high-B samples (0.8 < B < 0.9 *apfu*) are shown in Figure 14b with $^{M(1)}Fe^{2+}$ shown as a function of *T*(2)–O(7)–*T*(3) angle. There is a positive correlation between Fe^{2+} at *M*(1) and the *T*(2)–O(7)–*T*(3) angle, in agreement with the finding of Geisinger *et al.* (1985) that the chemical identity of a third cation bonded to the bridging O-atom can further influence *T*–O–*T* angles (*i.e.*, $^{M(1)}$Mg *versus* $^{M(1)}Fe^{2+}$). The perturbation in *T*(2)–O(7)–*T*(3) angles (Fig. 14a) is most obvious at high B (B > 0.8 *apfu*) because larger ranges in Fe^{2+} at *M*(1) only occur at a high content of boron (Table 7).

CONCLUSIONS

(1) The chemical formula of kornerupine may be written as $^{X}(\square,Mg,Fe^{2+})$ $^{M}(Al,Mg,Fe^{2+},Fe^{3+})_9$ $^{T}(Si,Al,B)_5 O_{21} (OH,F)$.

(2) In the forty-seven samples examined, the B content varies between 0.02 and 0.88 *apfu* and is completely ordered at the *T*(3) site.

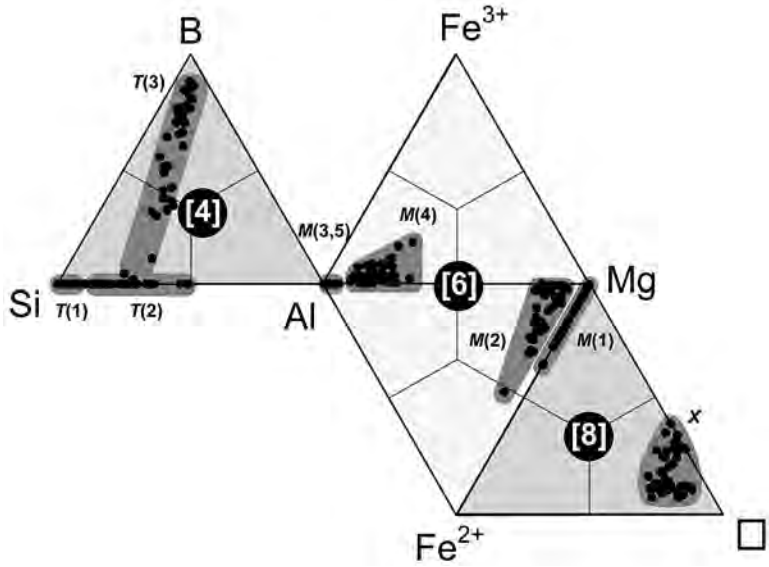

FIG. 12. Graphical summary of site occupancies in the kornerupine structures refined in this work. The *T*-site occupancies are shown within the B–Si–Al shaded triangle, the *M*-site occupancies are shown in the shaded Fe^{3+}–Al–Fe^{2+}–Mg diamond, and the *X*-site occupancies are shown in the shaded Mg–Fe^{2+}–□ triangle. Minor Ti^{4+}, V^{3+}, Cr^{3+} are included with Fe^{3+}, minor Mn^{2+} is included with Fe^{2+}, and minor Na and Ca are ignored.

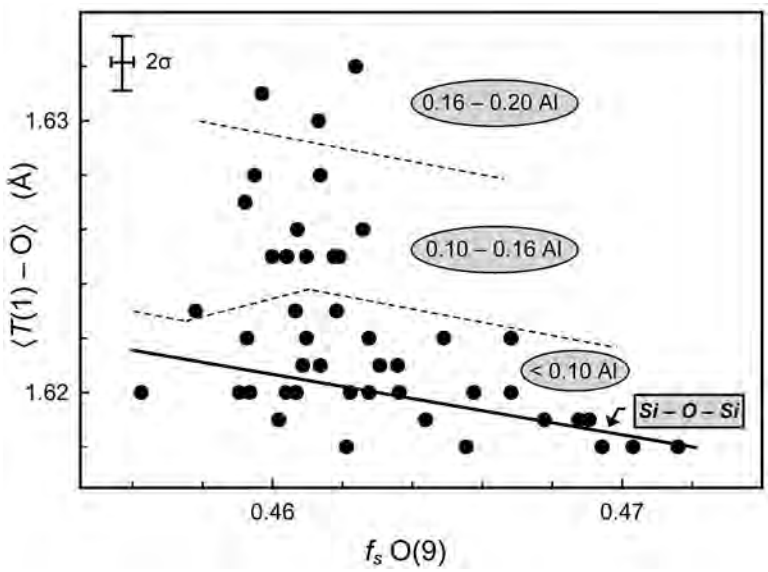

FIG. 13. Variation in <*T*(1)–O> (Å) *versus* f_s O(9) [1 / (1 – sec*TOT*)] in kornerupine. The *Si*–O–*Si* line is that of Geisinger *et al*. 1985 (solid line); dashed lines divide fields according to content of $^{T(1)}$Al *apfu*.

(3) All three *T* sites contain Si, with the site preference $T(1) > T(2) > T(3)$.

(4) There are very well-developed linear relations between <*T*–O> and $<r^{T}>$ at the three *T* sites.

(5) The *M*(1) site is occupied solely by Mg and Fe^{2+}, with $Mg > Fe^{2+}$.

(6) The *M*(2) site is occupied by Mg, Fe^{2+} and Al, with $(Mg \geq Fe^{2+}) > Al$.

(7) The *M*(3) and *M*(5) sites are occupied by Al and Mg with Al >> Mg.

(8) The *M*(4) site is occupied by Al, Mg, Fe^{3+} and minor transition elements, with $Al > Mg > Fe^{3+}$; Fe^{3+} is completely ordered at this site.

(9) There are well-developed linear relations between <*M*–O> and $<r^{M}>$ at the *M*(2), *M*(3), *M*(4) and *M*(5) sites.

(10) The <*M*(1)–O> distance is linearly related to $<r^{M(1)}>$ and the B content of the crystal; the latter influence is due to local steric strain.

(11) The *X* site is occupied by □, Mg, Fe^{2+} and minor Mn^{2+}, Na and Ca, with $□ > Mg \approx Fe^{2+}$.

(12) A radius for $^{X}□$ can be derived for kornerupine (1.045 Å). The <*X*–O> distance is linearly related to $<r^{X}>$ and the B and F contents of the crystal.

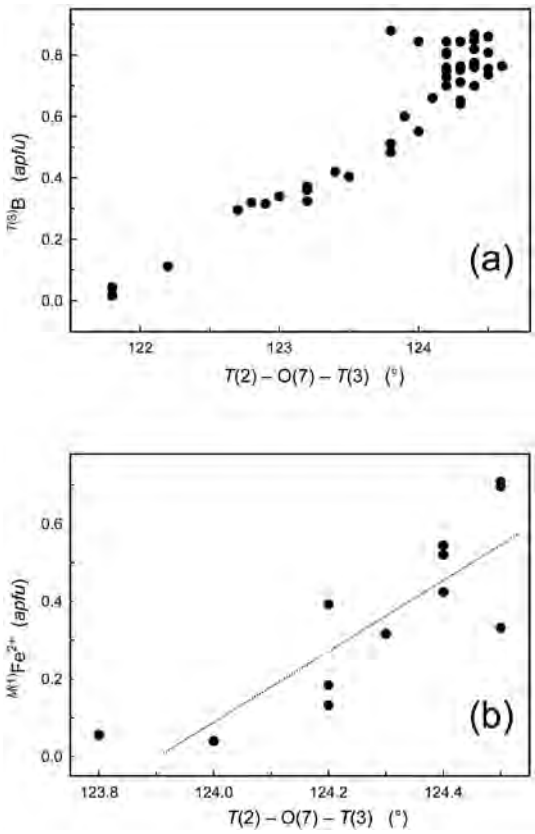

FIG. 14. Variation in selected site-populations in kornerupine: (a) $^{T(3)}$B (*apfu*) *versus* the *T*(2)–O(7)–*T*(3) angle (°); (b) $^{M(1)}$Fe^{2+} (*apfu*) *versus* T(2)–O(7)–*T*(3) (°) in crystals with $0.8 < B < 0.9$ *apfu*; the broken line passing through the data points is estimated by eye.

ACKNOWLEDGEMENTS

We thank Gianni Andreozzi, Sergio Lucchesi and Ron Peterson for their perspicacious comments on this paper. We also thank the following people and Institutions for samples: Carl Francis, Erik Jonsson, Juergen Malley, Duncan McKie, J.K. Nanda, P.H. Nixon, N.N. Pertsev, Ole Petersen, George Rossman, Douglas E. Thost, Julie K. Vry, R.G. Warren, D.J. Waters, D. Young, Adelaide University, American Museum of Natural History, British Museum of Natural History, Geologisk Museum (Copenhagen), Harvard University Mineralogical Museum, Institut für Mineralogie, Ruhr-Universität Bochum, Muséum National d'Histoire Naturelle, National Museum of Natural History, Smithsonian Institution, and the Royal Ontario Museum. Financial assistance was provided by Natural Sciences and Engineering Research Council of Canada grants to FCH.

REFERENCES

AZAVANT, P. & LICHANOT, A. (1993): X-ray scattering factors of oxygen and sulfur ions: an *ab initio* Hartree–Fock calculation. *Acta Crystallogr.* **A49**, 91-97.

BRAGA, R., CALLEGARI, A., MESSIGA, B., OTTOLINI, L., RENNA, M.R. & TRIBUZIO, R. (2003): Origin of prismatine from the Sondalo granulites (Central Alps, northern Italy). *Eur. J. Mineral.* **15**, 393-400.

COOPER, M.A., HAWTHORNE, F.C. & GREW, E.S. (2009b): The crystal chemistry of the kornerupine–prismatine series. V. The siting of beryllium in kornerupine. *Can. Mineral.* **47**, 303-313.

COOPER, M.A., HAWTHORNE, F.C., GREW, E.S. & ROSSMAN, G.R. (2009a): The crystal chemistry of the kornerupine–prismatine series. II. The role of hydrogen. *Can. Mineral.* **47**, 263-274.

FINGER, L.W. & HAZEN, R.M. (1981): Refinement of the crystal structure of an iron-rich kornerupine. *Carnegie Inst. Wash. Year Book* **80**, 370-373.

GEISINGER, K.L., GIBBS, G.V. & NAVROTSKY, A. (1985): A molecular orbital study of bond length and angle variations in framework structures. *Phys. Chem. Minerals* **11**, 266-283.

GREW, E.S. (1996): Borosilicates (exclusive of tourmaline) and boron in rock-forming minerals in metamorphic environments. *In* Boron: Mineralogy, Petrology and Geochemistry (E.S. Grew & L.M. Anovitz, eds.). *Rev. Mineral.* **33**, 387-502.

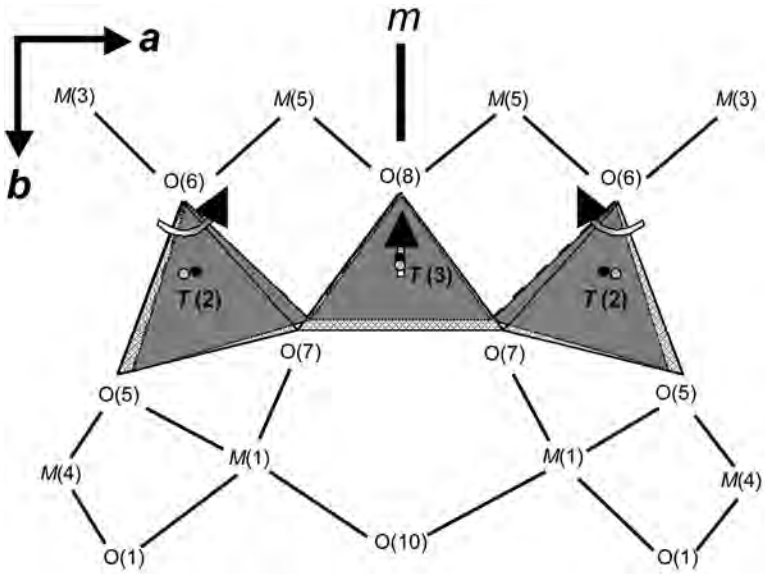

FIG. 15. The *T*(2)–*T*(3)–*T*(2) trimer of tetrahedra and neighboring environment in kornerupine, projected down [001]. K35 (low B) tetrahedra and corresponding *T*-sites are shaded light grey; K41 (high B) tetrahedra and corresponding *T*-sites are shaded dark grey and black, respectively. Arrows show the change from low B to high B content.

GREW, E.S., CHERNOSKY, J.V., WERDING, G., ABRAHAM, K., MARQUEZ, N. & HINTHORNE, J.R. (1990a): Chemistry of kornerupine and associated minerals, a wet chemical, ion microprobe, and X-ray study emphasizing Li, Be, B and F contents. *J. Petrol.* **31**, 1025-1070.

GREW, E.S., COOPER, M.A. & HAWTHORNE, F.C. (1996): Prismatine: revalidation for boron-rich compositions in the kornerupine group. *Mineral. Mag.* **60**, 483-491.

GREW, E.S., HERD, R.K. & MARQUEZ, N. (1987): Boron-bearing kornerupine from Fiskenæsset, West Greenland: a re-examination of specimens from the type locality. *Mineral. Mag.* **51**, 695-708.

GREW, E.S., LITVINENKO, A.K. & PERTSEV, N.N. (1990b): In search of whiteschists and kornerupine in the southwestern Pamirs, USSR. *Episodes* **13**, 270-274.

GREW, E.S., PERTSEV, N.N., VRÁNA, S., YATES, M.G., SHEARER, C.K. & WIEDENBECK, M. (1998): Kornerupine parageneses in whiteschists and other magnesian rocks: is kornerupine + talc a high-pressure assemblage equivalent to tourmaline + orthoamphibole? *Contrib. Mineral. Petrol.* **131**, 22-38.

GREW, E.S., REDHAMMER, G.J., AMTHAUER, G., COOPER, M.A., HAWTHORNE, F.C. & SCHMETZER, K. (1999): Iron in kornerupine: a ^{57}Fe Mössbauer spectroscopic study and comparison with single-crystal structure refinement. *Am. Mineral.* **84**, 536-549.

GREW, E.S., YATES, M.G., BERYOZKIN, V.I. & KITSUL, V.I. (1991a): Kornerupine in the slyudites from the Usmun River Basin in the Aldan Shield. 1. Geology and petrography. *Sov. Geol. Geophys.* **32**, 66-74.

GREW, E.S., YATES, M.G., BERYOZKIN, V.I. & KITSUL, V.I. (1991b): Kornerupine in the slyudites from the Usmun River Basin in the Aldan Shield. 2. Chemistry of the minerals, mineral reactions. *Sov. Geol. Geophys.* **32**, 85-98.

HAWTHORNE, F.C. (1983): The crystal chemistry of the amphiboles. *Can. Mineral.* **21**, 173-480.

HAWTHORNE, F.C., COOPER, M.A., BOTTAZZI, P., OTTOLINI, L., ERCIT, T.S. & GREW, E.S. (1995): Micro-analysis of minerals for boron by SREF, SIMS, and EMPA: a comparative study. *Can. Mineral.* **33**, 389-397.

HAWTHORNE, F.C., UNGARETTI, L., OBERTI, R., CAUCIA, F. & CALLEGARI, A. (1993a): The crystal chemistry of staurolite. I. Crystal structure and site populations. *Can. Mineral.* **31**, 551-582.

HAWTHORNE, F.C., UNGARETTI, L., OBERTI, R., CAUCIA, F. & CALLEGARI, A. (1993b): The crystal chemistry of staurolite. II. Order–disorder and the monoclinic → orthorhombic phase transition. *Can. Mineral.* **31**, 583-595.

HAWTHORNE, F.C., UNGARETTI, L., OBERTI, R., CAUCIA, F. & CALLEGARI, A. (1993c): The crystal chemistry of staurolite.

III. Local order and chemical composition. *Can. Mineral.* **31**, 597-616.

INTERNATIONAL TABLES FOR CRYSTALLOGRAPHY (1992). Vol. C. Kluwer Academic Publishers, Dordrecht, The Netherlands.

JONSSON, E. (1996): The first occurrence of a kornerupine-group mineral in Sweden: prismatine from Stakholmen, Hälsingland. *GFF* **118**, A52-A53.

KLASKA, R. & GREW, E.S. (1991): The crystal structure of B-free kornerupine: conditions favoring the incorporation of variable amounts of B through $^{[4]}B \rightleftharpoons {}^{[4]}Si$ substitution in kornerupine. *Am. Mineral.* **76**, 1824-1835.

MCKIE, D. (1965): The magnesium aluminum borosilicates: kornerupine and grandidierite. *Mineral. Mag.* **34**, 346-357.

MOORE, P.B. & ARAKI, T. (1979): Kornerupine: a detailed crystal-chemical study. *Neues Jahrb. Mineral., Abh.* **134**, 317-336.

MOORE, P.B. & BENNETT, J.M. (1968): Kornerupine: its crystal structure. *Science* **159**, 524-526.

MOORE, P.B., SEN GUPTA, P.K. & SCHLEMPER, E.O. (1989): Kornerupine: chemical crystallography, comparative crystallography, and its cation relation to olivine and to Ni_2In intermetallic. *Am. Mineral.* **74**, 642-655.

NIXON, P.H., GREW, E.S. & CONDLIFFE, E. (1984): Kornerupine in a sapphirine–spinel granulite from Labwor Hills, Uganda. *Mineral. Mag.* **48**, 550-552.

PETERSEN. O.V. & SECHER, K. (1993): The minerals of Greenland. *Mineral. Rec.* **24**(2).

POUCHOU, J.L. & PICHOIR, F. (1984): A new model for quantitative X-ray microanalysis. I. Application to the analysis of homogeneous samples. *La Recherche Aérosp.* **5**, 13-38.

POUCHOU, J.L. & PICHOIR, F. (1985): 'PAP' $\phi(\rho Z)$ procedure for improved quantitative microanalysis (J.T. Armstrong, ed.). *Microbeam Analysis*, 104-106.

SCHREYER, W. & ABRAHAM, K. (1976): Natural boron-free kornerupine and its breakdown products in a sapphirine rock of the Limpopo Belt, southern Africa. *Contrib. Mineral. Petrol.* **54**, 109-126.

SHANNON, R.D. (1976): Revised effective ionic radii and systematic studies of interatomic distances in halides and chalcogenides. *Acta Crystallogr.* **A32**, 751-767.

SMITH, J.V. (1954): A review of the Al–O and Si–O distances. *Acta Crystallogr.* **7**, 479-481.

SMITH, J.V. & BAILEY, S.W. (1963): Second review of Al–O and Si–O tetrahedral distances. *Acta Crystallogr.* **16**, 801-811.

SWANSON, D.K. (1980): *A Comparative Study of Ab Initio Generated Geometries for First and Second Row Atom Oxide Molecules with Corresponding Geometries in Solids*. M.S. thesis, Virginia Polytechnic Institute and State University, Blacksburg, Virginia.

SWANSON, D.K., MEAGHER, E.P. & GIBBS, G.V. (1980): Calculation of tetrahedral and octahedral bond lengths for third row elements. *Trans. Am. Geophys. Union.* **61**, 409 (abstr.).

VRY, J.K. (1994): Boron-free kornerupine from the Reynolds Range, Arunta Block, central Australia. *Mineral. Mag.* **58**, 27-37.

VRY, J.K. & CARTWRIGHT, I. (1994): Sapphirine–kornerupine rocks from the Reynolds Range, central Australia: constraints on the uplift history of a Proterozoic low pressure terrain. *Contrib. Mineral. Petrol.* **116**, 78-91.

WATERS, D.J. & MOORE, J.M. (1985): Kornerupine in Mg–Al-rich gneisses form Namaqualand, South Africa: mineralogy and evidence for metamorphic fluid actiivity. *Contrib. Mineral. Petrol.* **91**, 369-382.

WERDING, G. & SCHREYER, W. (1978): Synthesis and crystal chemistry of kornerupine in the system $MgO–Al_2O_3–SiO_2–B_2O_3–H_2O$. *Contrib. Mineral. Petrol.* **67**, 247-259.

YOUNG, D.A. (1995): Kornerupine-group minerals in Grenville granulite-facies paragneiss, Reading Prong, New Jersey. *Can. Mineral.* **33**, 1255-1262.

Received March 16, 2006, revised manuscript accepted March 20, 2009.

APPENDIX 1. REFINEMENT OF KORNERUPINE WITH IONIZED AND NEUTRAL SCATTERING-FACTORS FOR OXYGEN

Where cation site-scattering values at some sites are freely refined, the values scale to the scattering of the rest of the structure where the identity of the scattering species is known and fixed. The fixed part of the structure is commonly the anion component plus any cation component that is known to be ordered. The total scattering of the anion component of the structure is affected by the scattering factor(s) assigned to the anion species: neutral or ionized. As a result, the scattering values from the freely refined sites will be different depending on the ionization state of the scattering curves used for the anion species in the structure. The present work involves a large coherent dataset for a structure that shows significant variation in chemical composition, and the chemical compositions were carefully determined *via* electron-microprobe analysis and crystal-chemical analysis on the same grains. The data presented here are extremely coherent and provide an excellent opportunity to examine the effect of using different ionization states for the (fixed) anion species on the refined scattering values of the (variable) cation species in the structure.

We ran refinements for all 47 structures using the simplified refinement model described earlier in the text using (1) O^{2-} and (2) O-neutral scattering factors. The scattering factors used are shown in Table A1. In the structure of kornerupine, there are variable amounts of Fe^{2+} at the *X*, *M*(1) and *M*(2) sites, and Fe^{3+} orders at the *M*(4) site. Note that (Mg,Al) is dominant at these sites (12, 13 electrons), and the presence of Fe (26 electrons) increases in the refined site-scattering values. For both sets of refinements (O^{2-} *versus* O-neutral scattering factors), the total refined site-scattering over the [*X* + *M*(1) + *M*(2) + *M*(4)] sites is compared in Figure A1. The size of the data points approximates the cumulative site-scattering errors. Use of the O^{2-} scattering factor clearly results in a greater total refined scattering at these sites in all 47 refinements; the relative mean increase in cumulative site-scattering is ~1.1 *epfu* (electrons per formula unit). Careful inspection of Figure A1 also reveals that the departure of data from the 1:1 reference line is slightly greater for kornerupine crystals with greater Fe content. The most important chemical substitution at these sites involves Fe ⇌ (Mg,Al), and a 1.1 *epfu* difference implies a difference of ~0.08 *apfu* Fe ⇌ (Mg,Al), with the O^{2-} refinements indicating greater Fe contents at these sites. The higher refined site-scattering values obtained with the O^{2-} scattering factor are in closer agreement with the analogous electron counts derived from the formulae calculated from the electron-microprobe data. This is shown (using O^{2-}) by the even scatter about the 1:1 relation on the plot of refined site-scattering (SREF) *versus* the calculated scattering (EMPA) at the *X* site (Fig. 11d); note that there is a 1:1 relation between *epfu* from structure refinement and electron-microprobe analysis for all other sites [*M*(1), *M*(2), *M*(3), *M*(4), *M*(5), *T*(1), *T*(2), *T*(3)] prior to assignment of the scattering species at the *X* site.

TABLE A1. SCATTERING SPECIES AT EACH SITE IN THE REFINEMENT OF KORNERUPINE

Site	Scattering species*	Site	Scattering species*
X	Mg	*T*(1)	[Si]
M(1)	Mg	*T*(2)	[Si]
M(2)	Mg	*T*(3)	B,Si
M(3)	[Al]		
M(4)	Al	O(1→10)	[O^{0}] or [O^{2-}]
M(5)	[Al]	H	Not present

* square brackets denote fixed occupancy.

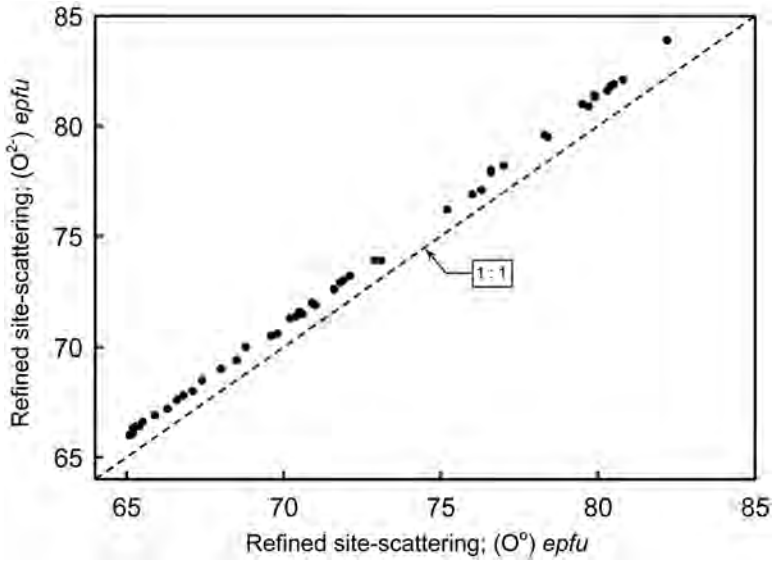

FIG. A1.

APPENDIX 2. KEY EXPRESSIONS

The form of the equations for the residual indices, extinction correction, and anisotropic-displacement parameters are as follows:

$R_1 = \Sigma(|F_o| - |F_c|) / \Sigma|F_o|$

$wR_2 = [\Delta w(F_o^2 - F_c^2)^2 / \Sigma w(F_o^2)^2]^{½}$

$w = 1/ [\sigma^2(F_o^2) + (a \times P)^2 + (b \times P)]$, where a and b are refineable parameters

$P = [\{\max(0,F_o^2)\} + 2F_c^2] / 3$

An extinction parameter X is refined, where

$F_c^* = kF_c [1 + 0.001 \times X \times F_c^2 \times \lambda^3 / \sin(2\theta)]^{-¼}$ (k is the overall scale-factor)

From the atom-displacement parameters:

for isotropic U: $\exp(-8\pi^2 U [\sin(\theta) / \lambda]^2$

for anisotropic U_{ij}: $\exp[-2\pi^2(h^2a^2U_{11} + k^2b^2U_{22} + l^2c^2U_{33} + 2hkabU_{12} + 2hlacU_{13} + 2klbcU_{23})]$, where U_{eq} is one-third of the trace of the orthogonalized U_{ij} tensor.